Assessment of Damköhler's hypotheses in the thin reaction zone regime using multi-step chemistry direct numerical simulations of statistically planar turbulent premixed flames

Cite as: Phys. Fluids **34**, 055120 (2022); https://doi.org/10.1063/5.0091979
Submitted: 19 March 2022 • Accepted: 21 April 2022 • Accepted Manuscript Online: 22 April 2022 • Published Online: 17 May 2022

H. S. Awad, K. Abo-Amsha, U. Ahmed, et al.

Physics of Fluids ARTICLE scitation.org/journal/phf

Assessment of Damköhler's hypotheses in the thin reaction zone regime using multi-step chemistry direct numerical simulations of statistically planar turbulent premixed flames

Cite as: Phys. Fluids **34**, 055120 (2022); doi: 10.1063/5.0091979
Submitted: 19 March 2022 · Accepted: 21 April 2022 ·
Published Online: 17 May 2022

View Online Export Citation CrossMark

H. S. Awad,[1] K. Abo-Amsha,[1] U. Ahmed,[1] M. Klein,[2,a)] and N. Chakraborty[1,b)]

AFFILIATIONS

[1]School of Engineering, Newcastle University, Claremont Road, Newcastle NE1 7RU, United Kingdom
[2]Department of Aerospace Engineering, University of the Bundeswehr Munich, Werner-Heisenberg-Weg 39, 85577 Neubiberg, Germany

Note: This paper is part of the special topic, Development and Validation of Models for Turbulent Reacting Flows.
[a)]**Author to whom correspondence should be addressed:** markus.klein@unibw.de
[b)]**Email:** nilanjan.chakraborty@ncl.ac.uk

ABSTRACT

The effects of the definition of the reaction progress variable and equivalence ratio on the validity of Damköhler's hypotheses for turbulent premixed flames belonging to the thin reaction zone regime have been studied using multi-step chemistry direct numerical simulations of statistically planar CH_4–air premixed flames with equivalence ratios of 0.8 and 1.0. Although CH_4–air premixed flames with equivalence ratios of 0.8 and 1.0 have effective Lewis numbers close to unity, local differential diffusion effects can play a non-negligible role in determining the turbulent burning velocity and flame surface area in all cases. However, the augmentations of burning rate and flame surface area under turbulence do not occur in equal proportion, but their ratio remains of the order of unity. This conclusion holds irrespective of the definition of the reaction progress variable for the cases considered here. Damköhler's second hypothesis, which relates the ratio of turbulent burning velocity and the unstretched laminar burning velocity to the ratio of turbulent diffusivity and molecular diffusivity, has been found not to hold in the sense of equality, but it is valid in an order of magnitude sense for all choices of reaction progress variable definition. The findings of the current analysis indicate that Damköhler's first and second hypotheses should only be interpreted in an order of magnitude sense in the thin reaction zone regime even when the effective Lewis number remains close to unity.

I. INTRODUCTION

Turbulent burning velocity S_T is a quantity of fundamental importance in the simulation and modeling of turbulent premixed combustion.[1–7] The turbulent burning velocity S_T is defined as[3]

$$S_T = (\rho_0 A_L)^{-1} \int_V \dot{w}_c dV, \tag{1}$$

where ρ_0 is the unburned gas density, A_L is the projected area in the direction of flame propagation, and $\dot{w}_c$ is the reaction rate of reaction progress variable c, which can be defined based on the mass fraction Y_α of a major species α as $c = (Y_{\alpha 0} - Y_\alpha)/(Y_{\alpha 0} - Y_{\alpha\infty})$ with subscripts 0 and ∞ referring to the values in the unburned gas and fully burned gas, respectively. The reaction rate $\dot{w}_c$ can be defined based on the species reaction rate $\dot{w}_\alpha$ and its mass fraction Y_α as $\dot{w}_c = -\dot{w}_\alpha/(Y_{\alpha 0} - Y_{\alpha\infty})$. Alternatively, a reaction progress variable can be defined based on temperature $\Theta = (T - T_0)/(T_{ad} - T_0)$ with T, T_0, and T_{ad} being the instantaneous temperature, unburned gas temperature, and adiabatic flame temperature, respectively. For high Damköhler number (i.e., $Da = lS_L/u'\delta_{th} \gg 1$) flames, Damköhler[1] suggested the following expression, which is commonly referred to as Damköhler's first hypothesis:[8,9]

$$S_T/S_L = A_T/A_L. \tag{2}$$

Here, A_T is the turbulent flame surface area, S_L is the unstretched laminar burning velocity, l is the integral length scale of turbulence, u' is the root mean square turbulent velocity fluctuation, and $\delta_{th} = (T_{ad} - T_0)/\max|\nabla T|_L$ is thermal flame thickness where the

subscript L refers to the values in the corresponding unstretched laminar premixed flame. Although Eq. (2) was proposed for $Da \gg 1$, it has been found that Eq. (2) holds well for statistically planar flames with unity Lewis number even for $Da < 1$ and for high values of Karlovitz number (i.e., $Ka = (u'/S_L)^{1.5}(l/\delta_{th})^{-0.5} \gg 1.0$).[8,10,11] The explanations for the validity of Eq. (2) for $Da < 1$ and $Ka > 1$ for statistically planar flames with unity Lewis number in the context of simple chemistry are provided elsewhere[9] and will not be repeated here. It has also been found that Eq. (2) holds reasonably well in the thin reaction zone regime[12] based on multi-step chemistry direct numerical simulation (DNS)[13,14] involving species with non-equal diffusivity for both hydrogen/air[13] and methane/air[14] flames. This contrasts with the experimental findings,[15–17] which revealed significant differences between S_T/S_L and A_T/A_L in the thin reaction zone regime. In this respect, it is worth noting that the length scale separation between integral length scale of turbulence and flame thickness in typical DNS studies[8,10,11,13,14] is severely limited when compared to the experimental investigations.[15–17] Moreover, a unity Lewis number condition is an idealization that is impossible to realize in an experimental condition. Furthermore, 3D experimental evaluation of displacement speed and flame area is not straightforward, which might give rise to additional uncertainties. It has also been demonstrated by Chakraborty *et al.*[9] that the evaluation of 2D quantities (as done in most experiments) and the presence of non-zero mean flame curvature can considerably amplify the discrepancy between S_T/S_L and A_T/A_L. Hence, it is not surprising that experimental observations regarding the validity of Eq. (2) can potentially differ from DNS analyses. Therefore, it is worthwhile to analyze the validity of Damköhler's first hypothesis [i.e., Eq. (2)] in the context of multi-step chemistry DNS to analyze the roles of the choice of reaction progress variable and the effects of preferential diffusion of different species on the validity of Eq. (2) in flames, which are characterized by a global Lewis number close to unity. This is one of the motivations behind the current analysis.

Damköhler[1] proposed another expression for S_T for small-scale turbulence (i.e., $l/\delta_{th} \ll 1$) characterized by $Da < 1$ in the following manner, which is commonly referred to as Damköhler's second hypothesis:[18,19]

$$S_T/S_L = \sqrt{D_t/D}, \tag{3}$$

where D_t and D are the turbulent diffusivity and molecular diffusivity of the reaction progress variable, respectively. The condition $l/\delta_{th} \ll 1$ has a limited practical relevance,[2,20,21] and thus, it is worthwhile to consider the validity of Eq. (3) in the low Damköhler number (i.e., $Da < 1$) thin reaction zone regime (i.e., $Ka > 1$)[12] of premixed turbulent combustion. A recent simple chemistry direct numerical simulation (DNS) analysis[22] revealed that $\sqrt{D_t/D}$ predicts S_T/S_L in an order of magnitude sense for the thin reaction zone regime premixed turbulent flames with $Da < 1$ provided D_t and D are evaluated at the leading edge of the flame brush. It is worth noting that the counter-gradient transport within the flame brush could make Eq. (3) invalid[19] but the gradient transport (thus a positive value of D_t) is realized at the leading edge even for flames where the counter-gradient transport is obtained within the flame brush,[22–24] and thus Eq. (3) can safely be applied at the leading edge of the flame brush. It is worth noting that Eq. (3) was also found to be valid in the context of G-equation DNS[25] and constant density DNS[26] in the past. This is consistent with experimental findings by Osborne *et al.*[27] who found that S_T/S_L remains proportional to $\sqrt{D_t/D}$ in the thin reaction zone regime. Therefore, it is worthwhile to investigate if the findings from G-equation DNS,[25] constant density DNS,[26] simple chemistry DNS,[22] and experimental[27] investigations remain valid in the context of multi-step skeletal chemistry DNS where the choice of reaction progress variable and preferential diffusion of species can potentially affect the validity of Eq. (3). This also serves another motivation for the current analysis.

The validity of both Eqs. (2) and (3) raises several questions in the context of multi-step chemical mechanisms. For example, the reaction progress variable c in a multispecies system can be defined in different ways, which is likely to affect $\dot{w}_c$ and therefore the magnitude of S_T. Moreover, the choice of c definition also affects the evaluation of turbulent flame surface area $A_T = \int_V |\nabla c| dV$[28] and the diffusivity of reaction progress variable D. Thus, both left- and right-hand sides of Eqs. (2) and (3) are likely to be affected by the choice of c. However, the effects of the definition of reaction progress variable on the validity of Damköhler's hypotheses [Eqs. (2) and (3)] are yet to be analyzed in the context of multispecies systems. To address this gap in the existing literature, a multi-step chemistry DNS database of statistically planar turbulent stoichiometric CH_4–air premixed flames with different turbulence intensities has been considered for the present analysis. Equations (2) and (3) do not make any assumption regarding the equivalence ratio ϕ, but ϕ can implicitly alter the global Lewis number and previous simple chemistry DNS revealed that non-unity global Lewis number alters the validity of Eq. (2).[29,30] Thus, to identify the effects of equivalence ratio ϕ on the validity of Eqs. (2) and (3), a DNS database of statistically planar CH_4–air flames with $\phi = 0.8$ has been considered beside $\phi = 1.0$, for the same set of initial values of u'/S_L and l/δ_{th} as that of the database for the stoichiometric CH_4–air premixed flames. This ensures that both $\phi = 0.8$ and 1.0 flames occupy the same location on the regime diagram[12] based on initial conditions. Bechtold and Matalon[31] proposed an expression for the effective Lewis number as follows: $Le_{eff} = 1 + \{(Le_{CH_4} - 1) + (Le_{O_2} - 1)A_{Le}\}/(1 + A_{Le})$ where $A_{Le} = 1 + \beta(\Phi - 1)$, $\beta = T_{ac}(T_{ad} - T_0)/T_{ad}^2$ is the Zel'dovich number and $\Phi = \max\{\phi, 1/\phi\}$ with T_{ac} being the activation temperature. The adiabatic flame temperatures T_{ad} for $\phi = 0.8$ and 1.0 for atmospheric methane–air combustion with $T_0 = 300$ K are 1996.9 and 2225.5 K, respectively. The activation temperature T_{ac} for methane–air combustion can be taken to be 15 900 K according to Tarrazo *et al.*,[32] which along with $Le_{CH_4} = 0.98$ and $Le_{O_2} = 1.10$ leads to $Le_{eff} = 1.07$ and 1.04 for $\phi = 0.8$ and 1.0, respectively. Thus, the effective Lewis number for the flames considered here remains close to unity, although ϕ can have an influence on Le_{eff}. This allows us for the analysis of the effects of ϕ on the validity of Damköhler's hypotheses under $Le_{eff} \approx 1.0$ conditions for which these hypotheses were found to be reasonably valid based on previous studies employing simple chemistry.[8–11,22] It has been demonstrated elsewhere[29,30] that Damköhler's first hypothesis is rendered invalid for flames with non-unity effective Lewis number. Thus, the choice of the range of ϕ considered in this study allows us for the analysis of the effects of ϕ on the validity of Damköhler's hypotheses under $Le_{eff} \approx 1.0$ conditions. Therefore, a significant departure of equivalence ratio in both $\phi < 0.8$ and $\phi > 1.0$ directions for methane–air mixture will change the effective Lewis number from unity for which at least the first hypothesis

becomes invalid[29,30] and thus $\phi < 0.8$ and $\phi > 1.0$ methane–air mixtures are not considered in this analysis.

Ahmed *et al.*[22] demonstrated, based on simple chemistry DNS with unity effective Lewis number, that Eqs. (2) and (3) are likely to be simultaneously valid at least for some ranges of u'/S_L and l/δ_{th} within the thin reaction zone regime (i.e., $Ka > 1$), and thus, the current analysis focuses on the thin reaction zone regime.[12] In this respect, the main objectives of the current analysis are as follows: (a) to assess the validity of both first and second hypotheses by Damköhler[1] in the presence of multi-step chemistry and transport, and (b) to identify the effects of equivalence ratio ϕ on the validity of Eqs. (2) and (3) in the thin reaction zone regime.

II. DNS DATABASE

The simulations have been conducted using a three-dimensional compressible DNS code SENGA2[33] where standard conservation equations of mass, momentum, internal energy, and species are solved in dimensional form. In SENGA2, all spatial derivatives are evaluated using the tenth-order central difference scheme for the internal grid points and the order of differentiation gradually drops to a fourth-order one-sided scheme at the non-periodic boundaries.[33] The time advancement has been achieved by an explicit fourth-order Runge–Kutta scheme. For the present analysis, a skeletal mechanism of CH_4–air combustion involving 16 species and 25 reactions[34] has been considered. The thermophysical properties such as viscosity, specific heat, and thermal conductivity have been taken to be temperature dependent and are computed using CHEMKIN polynomials.[33] The mixture-averaged transport model is used to account for molecular diffusion. The differences in species mass fractions in the unstretched laminar methane–air flames with $\phi = 0.8$ and 1.0 remain smaller than 1% between constant Lewis number and mixture-averaged transport assumptions, but here mixture-averaged transport is used for greater fidelity. The simulation domain is taken to be $20 \times 10 \times 10\,\text{mm}^3$, which is discretized by a uniform Cartesian grid of dimension $504 \times 252 \times 252$. The long side of the domain aligns with the mean direction of flame propagation, and the boundaries in this direction are taken to be partially non-reflecting. The transverse directions are taken to be periodic. The non-periodic boundary conditions are specified using the Navier–Stokes characteristic boundary condition (NSCBC) technique.[35] The reactive scalar field is initialized by the unstretched steady laminar flame solution, whereas turbulent velocity fluctuations are initialized by a well-known pseudo-spectral method.[36] For the present analysis, flame–turbulence interaction takes place under decaying turbulence. The initial values of $u'/S_L, l/\delta_{th}$, $Da = lS_L/u'\delta_{th}$, and $Ka = (u'/S_L)^{1.5}(l/\delta_{th})^{-0.5}$ are listed in Table I, and these conditions are also shown on the Borghi–Peters diagram in Fig. 1. It is worthwhile to note that the length scale ratio l/δ_{th} in this database remains small when compared with typical experimental analyses.[15–17] This is particularly important in terms of the assessment of Damköhler's first hypothesis, which was originally proposed for $l \gg \delta_{th}$. However, it was found to remain reasonably valid for moderate length scale separation in the thin reaction zone regime for flames with effective Lewis number close to unity.[8,10,11,13,14] The l/δ_{th} value considered here remains comparable to previous analyses[8,10,11,13,14] that discussed the validity of Damköhler's first hypothesis in the past. Damköhler's second hypothesis was proposed for small-scale turbulence (i.e., $l/\delta_{th} \ll 1$). The condition $l/\delta_{th} \ll 1$ has a limited practical relevance,[2,20,21] and thus, it is worthwhile to consider the validity of Eq. (3) in the low Damköhler number (i.e., $Da < 1$) thin reaction zone regime (i.e., $Ka > 1$)[12] of premixed turbulent combustion and the moderate value of l/δ_{th} for the DNS database considered here enables us to assess the validity of both first and second hypotheses by Damköhler simultaneously.

All these cases nominally belong to the thin reaction zone regime of combustion.[12] For these simulation parameters, at least ten grid points are kept within δ_{th}, and two grid points are accommodated within the Kolmogorov length scale η. The simulations have been conducted for $1.0\delta_{th}/S_L$ for $\phi = 0.8$, corresponding to $1.9\delta_{th}/S_L$ for $\phi = 1.0$, which amounts to $\{1.6, 2.5, 3.26\}t_e$ and $\{3.10, 4.65, 6.20\}t_e$ for $\phi = 0.8$ and 1.0, respective for initial $u'/S_L = \{4.0, 6.0, \text{and } 8.0\}$ with $t_e = l_0/\sqrt{k_0}$, l_0 and k_0 being the initial eddy turn over time, initial integral length scale of turbulence, and turbulent kinetic energy evaluated over the whole domain, respectively. The simulation time remains comparable to several previous DNS analyses,[8,19,37–40] and the temporal evolutions of S_T/S_L and the volume-averaged kinetic energy

TABLE I. Initial and final values of simulation parameters.

Parameters	Initial	Final ($\phi = 0.8$)	Final ($\phi = 1.0$)
u'/S_L	4.0, 6.0, 8.0	2.37, 3.02, 3.24	1.56, 1.66, 1.74
l/δ_{th}	3.0, 3.0, 3.0	3.04, 2.68, 2.81	3.36, 3.65, 3.95
Da	0.75, 0.5, 0.375	1.28, 0.89, 0.87	2.16, 2.20, 2.28
Ka	4.6, 8.5, 13.0	2.10, 3.21, 3.49	1.06, 1.12, 1.15

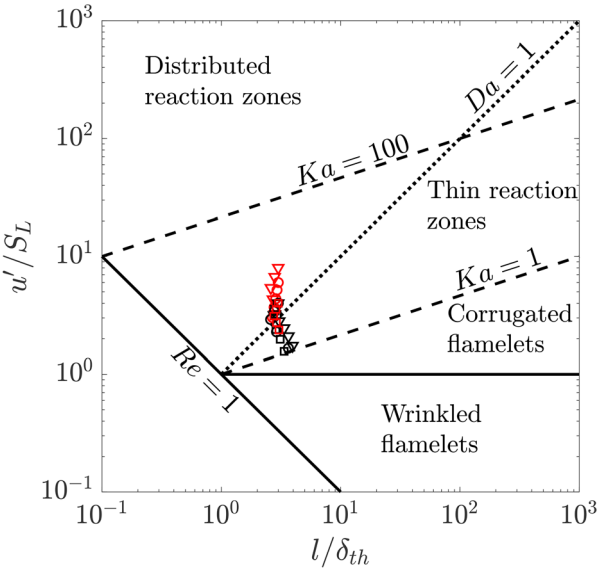

FIG. 1. Temporal evolution of the values of u'/S_L and l/δ_{th} on the Borghi–Peters diagram for $u'/S_L = 4.0$ (square), $u'/S_L = 6.0$ (circle), and $u'/S_L = 8.0$ (triangle) at $\phi = 0.8$ (red) and $\phi = 1.0$ (black). Note that values of u'/S_L decrease with increasing time, and the temporal range shown covers the range from the start till the end of the simulation. Please note that the initial state overlaps for both ϕ values.

normalized by its initial value k/k_0 for the cases considered here are shown in Fig. 2. It can be seen from Fig. 2 that both turbulent burning velocity and turbulent kinetic energy evaluated over the whole domain do not change rapidly with time when the statistics are extracted. The temporal evolutions of the cases considered here on the regime diagram are shown in Fig. 1. The values of u'/S_L and l/δ_{th} in the unburned gas ahead of the flame and the corresponding values of *Da* and *Ka* at the end of the simulation time are also listed in Table I. As the simulation time in terms of initial eddy turnover time t_e is greater for $\phi = 1.0$ than in the case of $\phi = 0.8$, the extent of decay of u'/S_L is greater for the $\phi = 1.0$ flames than for the $\phi = 0.8$ flames. Furthermore, stronger dilatation rate and thermal expansion effects in the $\phi = 1.0$ cases compared to $\phi = 0.8$ lead to more rapid decay of u'/S_L in the $\phi = 1.0$ flames. The statistics extracted at $1.0\,\delta_{th}/S_L$ for $\phi = 0.8$, which corresponds to $1.9\,\delta_{th}/S_L$ for $\phi = 1.0$, will be presented and discussed in Secs. III and IV, but the qualitative nature of these results remains unchanged halfway through the simulation time, which can be substantiated from the Appendix where the results for $\phi = 0.8$ and 1.0 cases are shown at $0.5\,\delta_{th}/S_L$ and $1.0\,\delta_{th}/S_L$, respectively. For the purpose of obtaining Reynolds/Favre averaging, the quantity in question is ensemble averaged over the statistically homogeneous directions (i.e., y and z directions in this analysis) at a given location in the direction of mean flame propagation (i.e., x direction) following previous analyses.[14,18,32–35]

III. ANALYSIS OF DAMKÖHLER'S FIRST HYPOTHESIS

The assessment of the validity of Damköhler's first hypothesis proceeds in three steps. The first subsection presents the normalized reaction rates and flame areas for the six different flames and for five different definitions of reaction progress based on CH_4, O_2, CO_2, and H_2O mass fractions as well as non-dimensional temperature Θ. Results will reveal that there is variation in the different normalized flame areas. The reasons for this will be explored in Secs. III B and III C.

A. Analysis of normalized reaction rate and normalized flame area

The instantaneous views of the non-dimensional temperature $\Theta = (T - T_0)/(T_{ad} - T_0) = 0.8$ isosurface at the time when statistics are extracted are shown in Fig. 3 for initial $u'/S_L = 4.0$, 6.0, and 8.0 for both $\phi = 0.8$ and 1.0. The maximum heat release rate for unstretched laminar premixed flames occurs close to $\Theta = 0.8$, and thus, the isosurfaces shown in Fig. 3 can be considered as the representative of the flame surface.

The OH-planar laser induced fluorescence (PLIF) method is often used to identify the reaction zone (i.e., taken to be the flame surface) in experimental investigations.[2,16,17,41–45] The OH-PLIF signal s_{OH} can be taken to be proportional to the mole fraction of OH (i.e., $s_{OH} \propto X_{OH} T^{-\beta_{OH}}$,[46] where X_{OH} is the mole fraction of OH and β_{OH} varies between -2.0 and 1.0, and is taken to be 0.0 here following Ref. 46). The OH-PLIF signal is sharpened further, without affecting the final result, using a numerical approximation of a Heaviside function in terms of $[s_{OH} - 0.2\ \{s_{OH}\}_L^{max}]$ (i.e., $H[s_{OH} - 0.2\{s_{OH}\}_L^{max}] = 0.5 + 0.5\tanh[k\{s_{OH} - 0.2\ \{s_{OH}\}_L^{max}\}]$ with $k \geq 10^6$) where $\{s_{OH}\}_L^{max}$ corresponds to the highest value of the OH-PLIF signal in the unstretched laminar premixed flame. The isosurfaces of $H[s_{OH} - 0.2\{s_{OH}\}_L^{max}] = 0.5$ are also superimposed on Fig. 3 on top of the $\Theta = 0.8$ isosurface. It is also evident from Fig. 3 that $H[s_{OH} - 0.2\{s_{OH}\}_L^{max}] = 0.5$ identifies a sharp interface between unburned reactants and fully burned products for all cases considered here (i.e., Θ ranges from 0.6 to 0.7 on the $H[s_{OH} - 0.2\{s_{OH}\}_L^{max}] = 0.5$ isosurface). Therefore, the interface given by $H[s_{OH} - 0.2\{s_{OH}\}_L^{max}] = 0.5$ can be considered to evaluate the turbulent flame surface area A_T^{OH}, as an alternative to the flame surface area evaluated by $A_T = \int_V |\nabla c| dV$.[28]

The variation of flame wrinkling with u'/S_L and ϕ can be quantified from the values of $\Omega = \int_V \dot{w}_c dV / \left[\int_V \dot{w}_c dV\right]_L$, $S = \int_V |\nabla c| dV / \left[\int_V |\nabla c| dV\right]_L$, and $S^{OH} = A_T^{OH}/A_L$, which are presented in Fig. 4 for different values of ϕ and u'/S_L at the time when the statistics are extracted, but the results corresponding to midpoint of the simulation

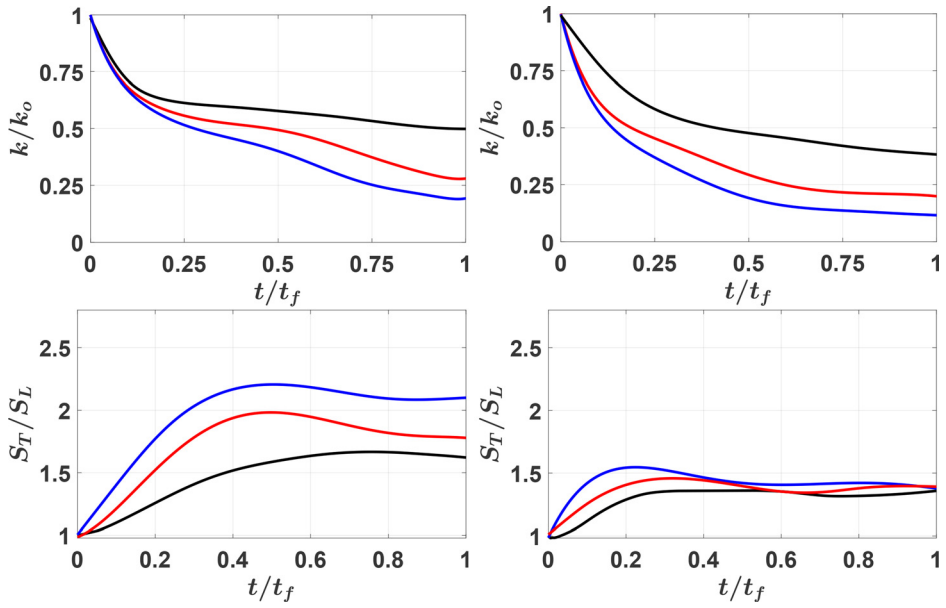

FIG. 2. Temporal evolutions of k/k_o (first row) and S_T/S_L (second row) for $\phi = 0.8$ and 1.0 (first to second column) for $u'/S_L = 4.0$ (black), $u'/S_L = 6.0$ (red), and $u'/S_L = 8.0$ (blue). Here, t_f is the chemical timescale (i.e., $t_f = \delta_{th}/S_L$) of the $\phi = 0.8$ mixture.

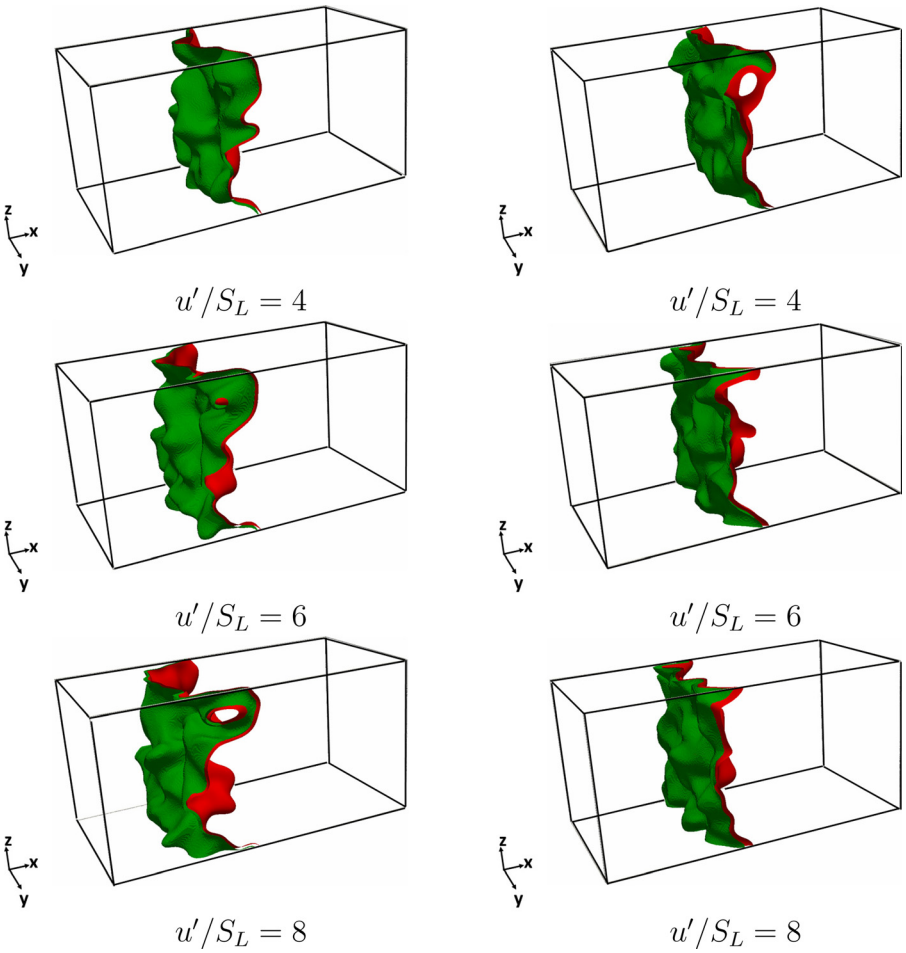

FIG. 3. Instantaneous views of $\Theta = 0.8$ isosurface (red) and $H[S_{OH} - 0.2\{S_{OH}\}_L^{max}] = 0.5$ isosurface (green) for different initial values of u'/S_L for $\phi = 0.8$ (first column) and $\phi = 1.0$ (second column) at the time when statistics were extracted (i.e., at $1.0\delta_{th}/S_L$ for $\phi = 0.8$, which corresponds to $1.9\delta_{th}/S_L$ for $\phi = 1.0$).

can be found in the Appendix. It is important to note here that the denominators in the definition of Ω and S can be expressed as $\left[\int_V \dot{w}_c dV\right]_L = \rho_0 S_L A_L$ and $\left[\int_V |\nabla c| dV\right]_L = A_L$, respectively, and these quantities are independent of the definition of reaction progress variable c. Here, A_L is the square cross-sectional area of the domain. For the evaluation of $S^{OH} = A_T^{OH}/A_L$, the turbulent flame surface area A_T^{OH} is evaluated using the surface area of the isosurfaces of $H[s_{OH} - 0.2\{s_{OH}\}_L^{max}] = 0.5$.[20,27,28,44,45] In Fig. 4, Ω and S values are shown for c definitions based on $\alpha = CH_4$, O_2, CO_2, and H_2O mass fractions. It can be seen from Fig. 4 that the choice of the species mass fraction for c definition does not significantly affect the values of Ω. However, the normalized flame surface area S for c definition based on H_2O mass fraction remains smaller than the corresponding values obtained from other definitions of reaction progress variable, and this trend is particularly prominent for high values of u'/S_L in the case of $\phi = 0.8$. The $c = 0.8$ isosurfaces based on O_2 mass fraction in both $\phi = 0.8$ and 1.0 are placed more toward the burned gas than the corresponding c isosurfaces based on H_2O mass fraction.[47] Thus, the reduced flame front wrinkling toward the burned gas side of the flame front[45,48,49] cannot be a possible explanation for reduced wrinkling of H_2O mass fraction-based c isosurfaces because S for O_2 mass fraction-based c is greater than the corresponding value for H_2O mass fraction-based c. The smaller extent of flame wrinkling for H_2O mass fraction-based c isosurfaces in comparison with the wrinkling of c isosurfaces based on alternative definitions of reaction progress variable was recently reported by Keil *et al.*[47] for $\phi = 1.0$ methane–air flames, but the same qualitative behavior has been observed here also for $\phi = 0.8$ flames. The detailed explanations for this behavior have been provided by Keil *et al.*,[47] which are not repeated here for the sake of conciseness, and interested readers are referred to Keil *et al.*[47] for further discussion in this regard. Moreover, in the context of multi-step chemistry and transport, it is possible to obtain superadiabatic temperature that leads to $\Theta > 1.0$ (especially for hydrogen-based fuels).[50] This precludes the usage of Θ as the reaction progress variable for general conditions. However, superadiabatic temperatures are not obtained for methane–air flames and thus the values of Ω and S are also shown here using $\Theta = c$ in this paper for the purpose of completeness. It can be seen from Fig. 4 that the results obtained for Θ-based reaction progress variable are both qualitatively and quantitatively similar to that for CH_4 mass fraction-based reaction progress variable.

B. Variation of local Lewis number

Figure 4 indicates that smaller values of Ω, S, and S^{OH} are obtained in the $\phi = 1.0$ case than in the $\phi = 0.8$ case. Previous

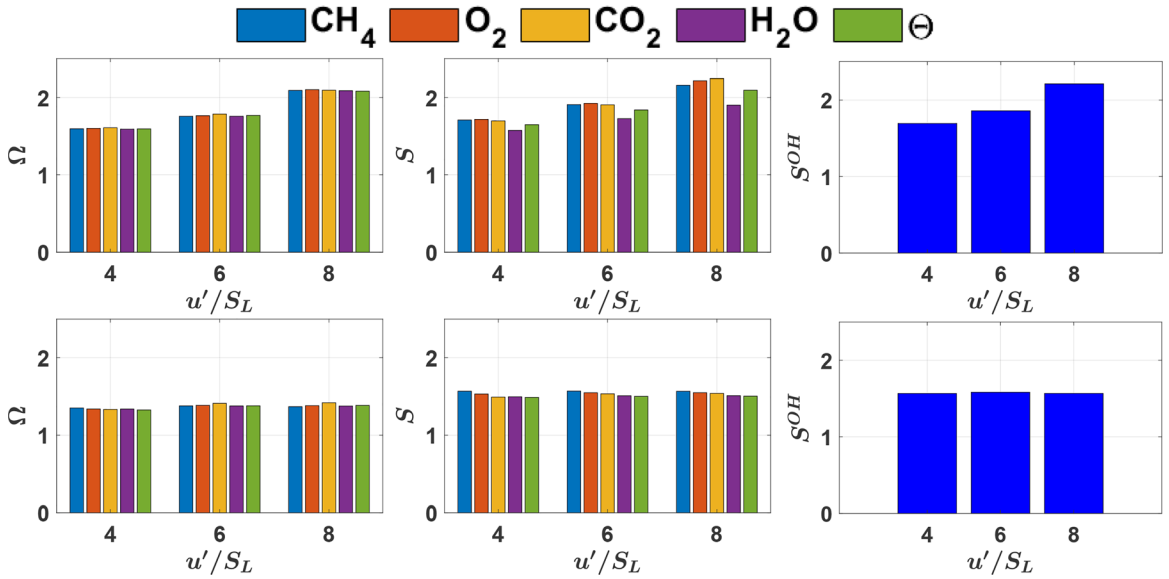

FIG. 4. Values of $\Omega = \int_V \dot{w}_c dV / \left[\int_V \dot{w}_c dV\right]_L$, $S = \int_V |\nabla c| dV / \left[\int_V |\nabla c| dV\right]_L$, and $S^{OH} = A_T^{OH}/A_L$ for c definitions based on CH_4, O_2, CO_2, and H_2O mass fractions and non-dimensional temperature Θ for different initial values of u'/S_L for both $\phi = 0.8$ and 1.0 (first to second row) at the time when statistics were extracted (i.e., at $1.0\delta_{th}/S_L$ for $\phi = 0.8$, which corresponds to $1.9\delta_{th}/S_L$ for $\phi = 1.0$).

theoretical,[51,52] experimental,[53] and computational[29,30,32,50,54] analyses based on simple chemistry revealed that the burning rate and flame wrinkling decrease with increasing global Lewis number, but these findings seem to contradict the present observations because $Le_{eff} = 1.07$ and 1.04 for $\phi = 0.8$ and 1.0, respectively, according to the effective Lewis number parameterization by Bechtold and Matalon.[31] In multi-step chemistry simulations, one global effective Lewis number might not be sufficient to define local differential diffusion effects. An alternative local effective Lewis number could be defined following Refs. 53 and 55 by including all species except nitrogen. This gives rise to $Le_V = \sum_{i=1}^{N-1} x_i' Le_i$ where $\sum_{i=1}^{N-1} x_i' = 1$ with x_i' are renormalized mole fractions for all species but excluding N_2, which does not participate in the reaction. Alternatively, a diffusion-based effective Lewis number can be defined as $Le_D = \left(\sum_{i=1}^{N-1} x_i'/Le_i\right)^{-1}$.[53,56] While these definitions are not meant to resolve the ambiguity in defining effective Lewis numbers, they provide a good impression of the changing molecular transport effects within the flame. The variations of Le_V and Le_D with CH_4 mass fraction-based reaction progress variable c for laminar 1D unstretched methane–air premixed flames with $\phi = 0.8$ and 1.0 are presented in Fig. 5, which shows that Le_V and Le_D assume values greater than 1.0 toward the unburned gas side of the flame but drop within the flame and take values smaller than unity within the flame in both cases, which is consistent with previous findings by Keil *et al.*[47] Differential diffusion effects potentially have an impact on the interrelation between reaction rate, curvature, and temperature, which in turn potentially changes the turbulent burning velocity and the flame area. This will be discussed next.

C. Differential diffusion effects on dependencies between curvature, reaction rate, and temperature

In order to explain this apparent contradiction related to flame surface area variation with Le_{eff}, the correlation coefficients between non-dimensional temperature $\Theta = (T - T_0)/(T_{ad} - T_0)$ and flame curvature $\kappa_m = 0.5\nabla \cdot \vec{N} = 0.5\nabla \cdot (-\nabla c/|\nabla c|)$ for the $c = 0.8$ iso-surface are shown in Fig. 6 (left) for c definitions based on CH_4, O_2, CO_2, and H_2O mass fractions. For these definitions, κ_m assumes positive (negative) values for the flame elements convex (concave) toward the reactants, and the flame normal vector $\vec{N} = -\nabla c/|\nabla c|$ points toward the reactants. It can be inferred from Fig. 6 (left) that for c definitions based on CH_4, O_2, CO_2 mass fractions, high

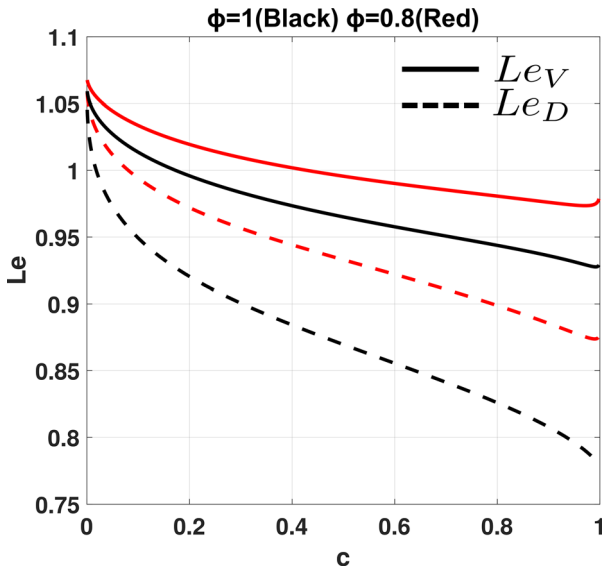

FIG. 5. Variation of Le_V and Le_D with CH_4 mass fraction-based reaction progress variable c for 1D unstretched laminar premixed flame with $\phi = 0.8$ and 1.0.

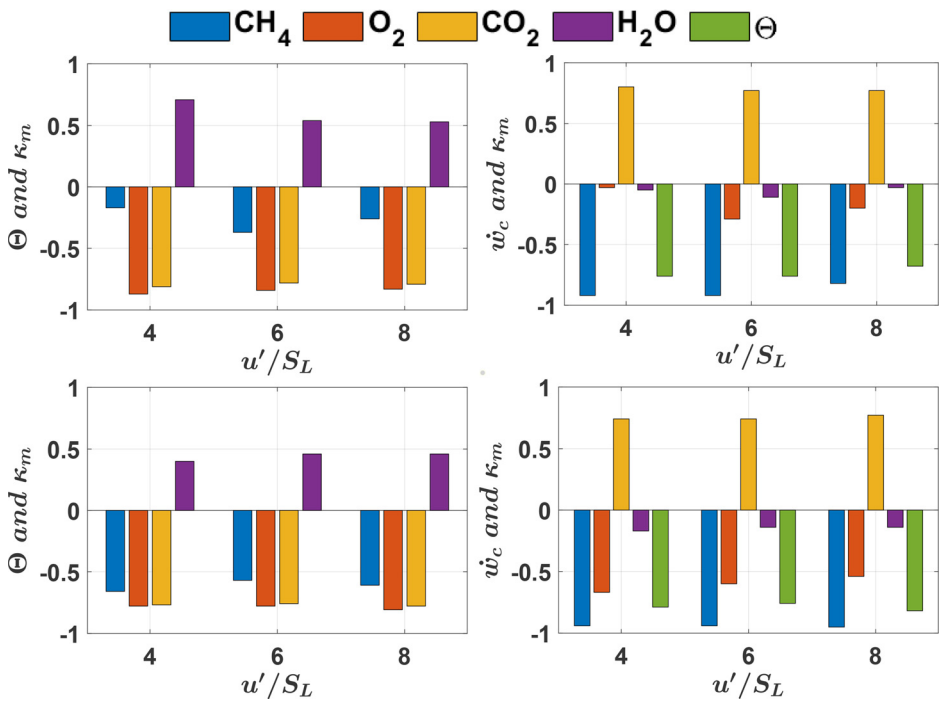

FIG. 6. Correlation coefficients between Θ and κ_m for $c = 0.8$ isosurface based on CH_4, O_2, CO_2, and H_2O mass fractions (first column) and correlation coefficients between $\dot{w}_c$ and κ_m for $c = 0.8$ isosurface based on CH_4, O_2, CO_2, and H_2O mass fractions and non-dimensional temperature Θ (for which $\dot{w}_c = \dot{w}_\Theta$ is considered) (second column) for different initial values of u'/S_L for both $\phi = 0.8$ and 1.0 (first and second row) at the time when statistics were extracted (i.e., at $1.0\delta_{th}/S_L$ for $\phi = 0.8$, which corresponds to $1.9\delta_{th}/S_L$ for $\phi = 1.0$).

(low) Θ values are associated with the regions that are concave (convex) to the reactants, which can be confirmed from Fig. 7 where the $c = 0.8$ isosurfaces colored by local values of Θ are shown for different definitions of reaction progress variable exemplarily for the initial

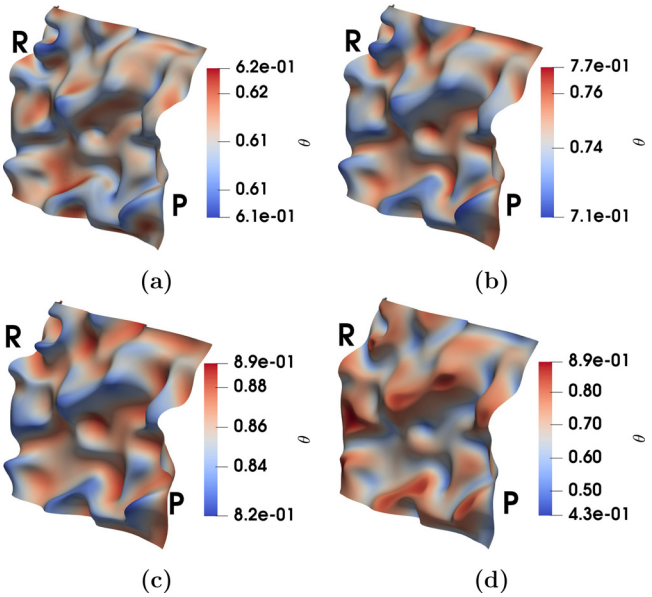

FIG. 7. Local distribution of non-dimensional temperature Θ on the $c = 0.8$ isosurface for reaction progress variable definitions based on CH_4(a), O_2 (b), CO_2 (c), and H_2O (d) mass fractions for the initial $u'/S_L = 4.0$ case with $\phi = 0.8$. The isosurfaces face the reactant side in these figures. The reactant and product sides are indicated by "R" and "P," respectively, in these figures.

$u'/S_L = 4.0$ case with $\phi = 0.8$. This behavior is qualitatively similar to those observed for simple chemistry DNS for $Le_{eff} > 1.0$.[29,50,54] It is more prominent for the $\phi = 1.0$ cases than in the $\phi = 0.8$ cases for the CH_4 mass fraction-based $c = 0.8$ isosurface with the negative correlation between Θ and κ_m being stronger in the $\phi = 1.0$ case than in the $\phi = 0.8$ case.

The defocusing rates of OH ($Le_{OH} = 0.73$) and heat from the burned gas region at the positively curved locations take place at a faster rate than the rate of diffusion of CO ($Le_{CO} = 1.10$), and thus, the heat release rate due to $CO + OH \rightarrow CO_2 + H$ remains small in these regions. This further reduces the subsequent methane consumption due to $CH_4 + H \rightarrow CH_3 + H_2$. However, the forward reaction rate of $CH_4 + H \rightarrow CH_3 + H_2$ is endothermic, and so, the combination of reduced magnitudes of exothermic $CO + OH \rightarrow CO_2 + H$ reaction and endothermic $CH_4 + H \rightarrow CH_3 + H_2$ (with a one order of magnitude smaller heat release) reaction gives rise to low temperature on the positively curved locations for c definitions based on CH_4, O_2, CO_2 mass fractions. This can be verified from Fig. 8 where the local distributions of the mass fractions of OH, CO, CO_2, H and heat release rate for $CO + OH \rightarrow CO_2 + H$ and $CH_4 + H \rightarrow CH_3 + H_2$ are shown on the $c = 0.8$ isosurface based on CH_4 mass fraction exemplarily for initial $u'/S_L = 4.0$ case with $\phi = 0.8$. The same qualitative behavior is obtained for O_2 and CO_2 mass fraction-based c isosurfaces and for $\phi = 1.0$, which are not explicitly shown here for the sake of brevity.

Figure 8 shows that the concentrations of OH and H indeed remain small at the positively curved locations, whereas CO concentration assumes high values at these zones. It can further be seen from Fig. 8 that the heat release rate of the exothermic $CO + OH \rightarrow CO_2 + H$ remains one order of magnitude greater than the negative heat release for $CH_4 + H \rightarrow CH_3 + H_2$ at the positively curved

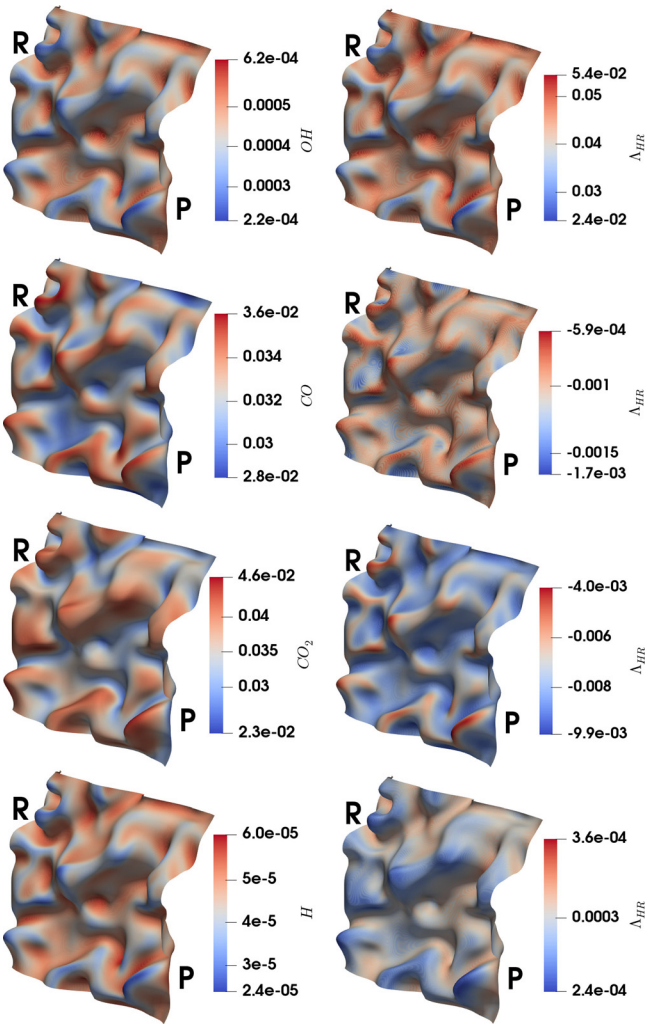

FIG. 8. Distributions of mass fractions of OH, CO, CO_2, and H (first column) and normalized heat release rate $\Lambda_{HR} = HR \times \delta_{th}/[\rho_0 C_{P0} S_L(T_{ad} - T_o)]$ (second column) for $CO + OH \rightarrow CO_2 + H$ (first row), $CO_2 + H \rightarrow CO + OH$ (second row), $CH_4 + H \rightarrow CH_3 + H_2$ (third row), and $CH_3 + H_2 \rightarrow CH_4 + H$ (fourth row) on the $c = 0.8$ isosurface based on CH_4 mass fraction for the initial $u'/S_L = 4.0$ case with $\phi = 0.8$. Here, *HR* is the heat of reaction for the reaction step in question and C_{P0} is the unburned gas-specific heat. The isosurfaces face the reactant side in these figures. The reactant and product sides are indicated by R and P, respectively, in these figures.

locations and thus the reduced temperature at these locations is principally influenced by $CO + OH \rightarrow CO_2 + H$. The focusing rates of OH and heat at the negatively curved locations are faster than the diffusion rate of CO, and thus, the heat release rate due to the exothermic reaction of $CO + OH \rightarrow CO_2 + H$ and the methane consumption by the endothermic reaction of $CH_4 + H \rightarrow CH_3 + H_2$ remains relatively high in these regions. It can indeed be seen from Fig. 8 that the concentrations of OH and H are relatively high at the negatively curved locations, whereas CO concentration remains relatively small at these zones. Moreover, the magnitude of negative heat release rate due to the endothermic reaction $CH_4 + H \rightarrow CH_3 + H_2$ remains small in comparison with relatively high heat release rate due to the exothermic $CO + OH \rightarrow CO_2 + H$ reaction at the negatively curved locations. This leads to negative correlations between Θ and κ_m for *c* definitions based on CO_2, O_2, and CH_4 mass fractions. It can be seen from Fig. 6 (left) that negative correlations between Θ and κ_m in the case of O_2 and CO_2 mass fraction-based $c = 0.8$ isosurfaces are marginally stronger in the $\phi = 0.8$ case than in the $\phi = 1.0$ case, which is consistent with previous simple chemistry DNS[29,30,50] and analytical[51,52] findings indicating that stronger negative correlations between Θ and κ_m are obtained for higher values of Le_{eff}. The CO concentration remains relatively small in the $\phi = 0.8$ cases compared to the $\phi = 1.0$ cases, and thus, the preferential diffusion (i.e., $Le > 1$) effects induced by CO ($Le_{CO} = 1.1$) remain weak for the $\phi = 0.8$ flames. Furthermore, Fig. 2 and Table I show that u'/S_L values remain greater in the $\phi = 0.8$ cases than in the $\phi = 1.0$ cases when statistics are extracted and the higher turbulence intensities for the $\phi = 0.8$ cases also act to reduce the correlation strength between Θ and κ_m. The combination of these gives rise to weaker correlation between Θ and κ_m for the CH_4 ($Le_{CH_4} = 0.97$) mass fraction-based reaction progress variable in the $\phi = 0.8$ cases in comparison with the $\phi = 1.0$ cases. It can be seen from Fig. 5 that Le_V and Le_D values remain closer to unity for the $\phi = 0.8$ cases than in the $\phi = 1.0$ cases and for the unity Lewis number no correlation is expected between Θ and κ_m;[29,30,50–52] this is consistent with the weaker correlation between Θ and κ_m for the CH_4 ($Le_{CH_4} = 0.97$) mass fraction-based reaction progress variable in the $\phi = 0.8$ cases than in the $\phi = 1.0$ cases.

A positive correlation between Θ and κ_m is obtained for the H_2O mass fraction-based reaction progress variable, and this positive correlation is stronger for $\phi = 0.8$ flames. It was explained by Keil *et al.*[47] that positively curved regions of the $c = 0.8$ isosurface based on H_2O mass fraction reach less into the unburned gas side due to its smaller extent of wrinkling than the corresponding temperature isosurface (because of higher mass diffusivity than thermal diffusivity), and hence, they are characterized by higher temperatures. Similarly, negatively curved regions of the $c = 0.8$ isosurface based on H_2O mass fraction reach less into the burned gas side and are consequently characterized by lower temperatures. Moreover, it was demonstrated by Keil *et al.*[47] that the focusing of O ($Le_O = 0.7$) from the unburned gas side at the positively curved locations of the $c = 0.8$ isosurface based on H_2O mass fraction takes place at a faster rate than the defocusing of H_2O ($Le_{H_2O} = 0.83$) and heat from the burned gas side and this gives rise to a higher likelihood of the endothermic reaction $O + H_2O \rightarrow OH + OH$, which promotes heat release due to exothermic $CO + OH \rightarrow CO_2 + H$ reaction. This can be verified from Fig. 9 where the local distributions of the mass fractions of OH, O and heat release rate for $CO + OH \rightarrow CO_2 + H$ and $O + H_2O \rightarrow OH + OH$ are shown on the $c = 0.8$ isosurface based on H_2O mass fraction exemplarily for initial $u'/S_L = 4.0$ case with $\phi = 0.8$. The same qualitative behavior is obtained for other values of ϕ and u'/S_L, which are not explicitly shown here for the sake of brevity. The higher magnitudes of endothermic $O + H_2O \rightarrow OH + OH$ and exothermic $CO + OH \rightarrow CO_2 + H$ reactions can be seen at the positively curved zones in Fig. 9 alongside high concentrations of OH, O, and CO_2 and low concentration of CO in these regions. This combination increases the temperature at the positively curved zones on the H_2O mass fraction-based reaction progress variable isosurfaces because positive heat release rate of $CO + OH \rightarrow CO_2 + H$ remains greater

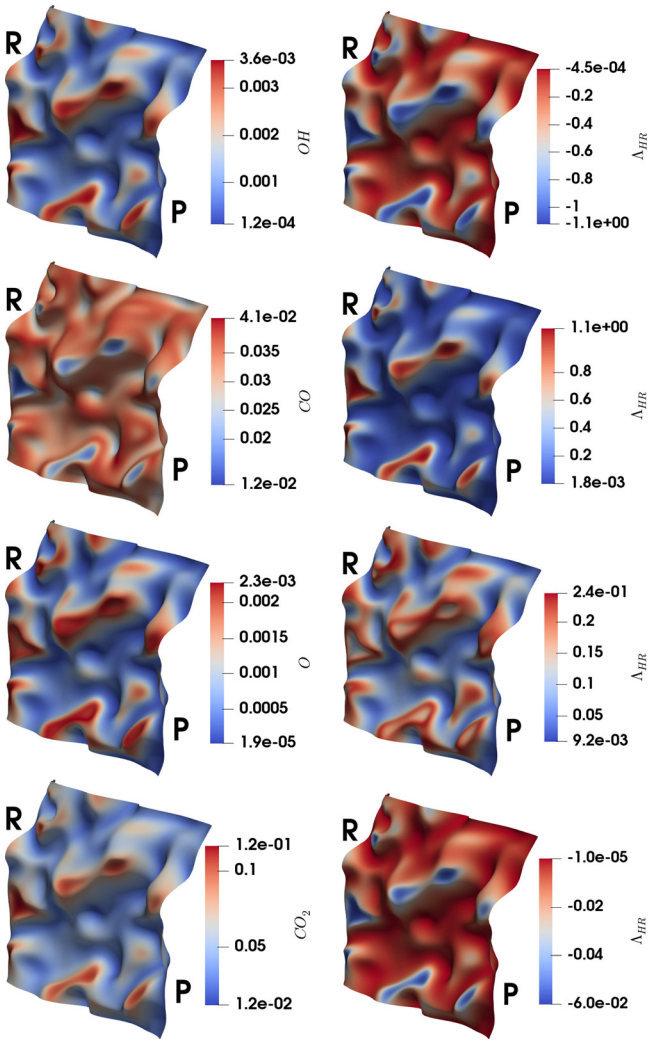

FIG. 9. Distributions of mass fractions of OH, CO, O, and CO_2 (first column) and normalized heat release rate $\Lambda_{HR} = HR \times \delta_{th}/(\rho_O C_{P_O} S_L (T_{ad} - T_o))$ (second column) for $O + H_2O \rightarrow OH + OH$ (first row), $OH + OH \rightarrow O + H_2O$ (second row), $CO + OH \rightarrow CO_2 + H$ (third row), and $CO_2 + H \rightarrow CO + OH$ (fourth row) on the $c = 0.8$ isosurface based on H_2O mass fraction for the initial $u'/S_L = 4.0$ case with $\phi = 0.8$. Here, *HR* is the heat of reaction for the reaction step in question and C_{P0} is the unburned gas-specific heat. The isosurfaces face the reactant side in these figures. The reactant and product sides are indicated by R and P, respectively, in these figures.

than negative heat release rate due to $O + H_2O \rightarrow OH + OH$. The higher likelihood of $O + H_2O \rightarrow OH + OH$ reaction due to high O concentration at the positively curved zones also decreases the wrinkling of H_2O mass fraction-based progress variable isosurface at the positively curved locations, whereas just the opposite mechanisms lead to less wrinkling and smaller temperatures in the negatively curved locations. Interested readers are referred to Keil *et al.*[47] for a detailed discussion, and the same qualitative behavior has been observed here also for $\phi = 0.8$ and 1.0 cases considered here (not shown here for brevity).

It is important to note that the reaction rate $\dot{w}_c$ in multi-step chemistry is not only dependent on temperature and thus the correlation between $\dot{w}_c$ and κ_m can be different from the correlation between Θ and κ_m. It can be seen from Fig. 6 (right) that the correlation between $\dot{w}_c$ and κ_m remains negative for c definitions based on CH_4, O_2, and H_2O mass fractions in all cases irrespective of the value of u'/S_L and ϕ. The correlation between $\dot{w}_\Theta = \dot{w}_T/(h_b - h_u)$ (where $\dot{w}_T, h_u$, and h_b are the heat release rate, sensible enthalpies in the unburned gas, and fully burned products, respectively) and κ_m has also been found to be qualitatively similar to that of the correlation between $\dot{w}_c$ and κ_m for CH_4 mass fraction-based reaction progress variable. These findings from Fig. 6 (right) are also consistent with previous findings by Keil *et al.*[47] for $\phi = 1.0$ methane–air flames. A positive correlation between $\dot{w}_c$ and κ_m is obtained for c definition based on CO_2 mass fraction in all cases irrespective of the value of u'/S_L and ϕ. The negative activation energy allows for $CO + OH \rightarrow CO_2 + H$[34] to proceed even at the relatively low-temperature positively curved locations. The weak focusing rate of CO_2 at the high-temperature negatively curved locations (see qualitative nature of CO_2 distribution in Fig. 8) promotes the backward reaction $CO_2 + H \rightarrow CO + OH$. The combined effect of these mechanisms is reflected in a positive correlation between $\dot{w}_c$ and κ_m for the CO_2 mass fraction-based reaction progress variable. At the positively curved locations on the H_2O mass fraction-based reaction progress variable, focusing of O ($Le_O = 0.7$) takes place at a faster rate than the defocussing of H_2O ($Le_{H_2O} = 0.83$) and heat and this gives rise to a higher likelihood of the reaction $O + H_2O \rightarrow OH + OH$ (see Fig. 9), which in turn promotes a negative correlation between $\dot{w}_c$ and κ_m despite a positive correlation between Θ and κ_m. These two counter-acting effects partially cancel each other to yield a weak correlation between $\dot{w}_c$ and κ_m for H_2O mass fraction-based reaction progress variable in comparison with those observed for O_2 and CO_2 mass fraction-based reaction progress variables. The concentrations of O and H_2O remain smaller in the $\phi = 0.8$ cases than in the $\phi = 1.0$ cases, and thus, the differential diffusion effects induced by O and H_2O are expected to be stronger in the $\phi = 1.0$ cases, which are reflected in the stronger negative correlation between $\dot{w}_c$ and κ_m for H_2O mass fraction-based reaction progress variable for $\phi = 1.0$ cases. This is consistent with the Le_V and Le_D values within the flame remaining closer to unity in the $\phi = 0.8$ methane–air flames than in the case of the $\phi = 1.0$ methane–air flames (see Fig. 5), and thus, the differential diffusion effects are weaker in the $\phi = 0.8$ methane–air flames, which are also reflected in the weaker negative correlation between $\dot{w}_c$ and κ_m for O_2 mass fraction-based $c = 0.8$ isosurface in the $\phi = 0.8$ cases than in the $\phi = 1.0$ cases. The higher turbulence intensities in the $\phi = 0.8$ cases than in the $\phi = 1.0$ cases (see Table I) also act to weaken this correlation. The negative correlation between $\dot{w}_c$ and κ_m for O_2 ($Le_{O_2} = 1.10$) mass fraction-based $c = 0.8$ isosurface is consistent with previous simple chemistry analyses,[29,30,54] which predicted a negative correlation when the Lewis number of reaction progress variable is greater than unity.

The above discussion indicates that a single global effective Lewis number Le_{eff} may not be sufficient for explaining the trends originating from local differential diffusion of intermediate species. It can be seen from Table I that $\phi = 1.0$ cases are subjected to weaker final turbulence than in $\phi = 0.8$ cases, and the Karlovitz number values of $\phi = 0.8$ cases remain greater than those for $\phi = 1.0$ cases when the statistics were extracted. Thus, the effective value of Lewis number cannot be considered in isolation to explain the observed trends of

Ω, S, and S^{OH} for the cases considered here. The stronger turbulence intensity u'/S_L and higher Ka in $\phi = 0.8$ cases than in $\phi = 1.0$ cases also contribute to higher values of Ω, S, and S^{OH} in $\phi = 0.8$ cases. Finally, it is worth remarking here that the correlation coefficients presented in Fig. 6 are not sensitive to u'/S_L variations within the parameter range considered here, but a larger range of parameters needs to be explored to make a more definite claim in this regard.

Figure 10 shows the values of $T_I = \Omega/S$ and $T_I^{OH} = \Omega/S^{OH}$ for c definitions based on CH_4, O_2, CO_2, and H_2O mass fractions, which reveals that both T_I and T_I^{OH} remain comparable and of the order of unity. However, T_I remains smaller than 1.0 (up to 14% for CH_4) irrespective of the definition of c for the $\phi = 1.0$ cases. This remains valid also for c definitions based on CH_4, O_2, CO_2 mass fractions, and a qualitatively similar result can be obtained if c is defined based on the non-dimensional temperature Θ. The term T_I assumes a value close to but smaller than 1.0 for initial $u'/S_L = 4.0$ and 6.0 cases, whereas T_I remains greater than 1.0 in particular for initial $u'/S_L = 8.0$ in the case of $\phi = 0.8$ when c is defined based on H_2O mass fraction.

A unity value of T_I and T_I^{OH} is indicative of the validity of Eq. (2), and thus, Fig. 10 shows that the left-hand side and right-hand side of Eq. (2) are not equal in the cases considered here despite Le_{eff} for these cases remaining close to unity. This is consistent with recent multi-step chemistry DNS findings by Attili *et al.*,[14] which revealed that $T_I = (S_T/S_L)/(A_T/A_L)$ does not remain unity but assumes a value close to unity (ranging from 1.0 to 1.4) for a configuration, which has a negative mean curvature. It was discussed by Chakraborty *et al.*[9] that S_T/S_L is expected to assume greater values than that of A_T/A_L under the unity Lewis number assumption for flames with negative mean curvature, and just the opposite behavior is expected for configurations with positive mean curvature, which was demonstrated recently by Ozel-Erol *et al.*[54] However, values of T_I and T_I^{OH} for the cases considered here remain mostly smaller than unity (see Fig. 10) although these flames are statistically planar (i.e., mean curvature remains vanishingly small). Moreover, both T_I and T_I^{OH} assume smaller values in the $\phi = 1.0$ cases than in the $\phi = 0.8$ cases. The smaller variation of T_I^{OH} can be explained by the small variation of Ω values (see Fig. 4) combined with division by the identical flame surface area S^{OH}. The sub-unity values of T_I and T_I^{OH} are consistent with previous findings for simple chemistry results when the diffusion rate of heat supersedes the species diffusion rate [24,25,41,42] (i.e., $Le_{eff} > 1.0$). In order to explain this behavior, it is worthwhile to consider the following identity based on the definition of displacement speed:[2,24,25,32]

$$[\dot{w}_c + \nabla \cdot (\rho D \nabla c)] = \rho S_d |\nabla c|, \tag{4}$$

where $S_d = (Dc/Dt)/|\nabla c|$ is the displacement speed. On volume-integrating Eq. (4) on both sides, one obtains

$$\int_V \dot{w}_c dV = \int_V \rho S_d |\nabla c| dV = \langle \rho S_d \rangle_V A_T, \tag{5}$$

where $\int_V \nabla \cdot (\rho D \nabla c) dV = 0$, because of the divergence theorem, $A_T = \int_V |\nabla c| dV$ is the flame surface area and $\langle \rho S_d \rangle_V$ is given by $\langle \rho S_d \rangle_V = \int_V \rho S_d |\nabla c| dV / \int_V |\nabla c| dV$. It can be appreciated from Eq. (5) that Eq. (2) holds when $\langle \rho S_d \rangle_V = \rho_0 S_L$ because $\left[\int_V \dot{w}_c dV\right]_L = \rho_0 S_L A_L$. For statistically planar flames, $\langle \kappa_m \rangle_V = \int_V \kappa_m |\nabla c| dV / \int_V |\nabla c| dV$ remains negligible and the effects of high values of reaction rate at the negatively curved locations tend to nullify (note that $\dot{w}_c$ has a non-linear curvature dependence and thus does not fully nullify) those of the reduced $\dot{w}_c$ values at the positively curved locations for c definitions based on CH_4, O_2, and H_2O mass fractions (see Fig. 4). By contrast, high values of reaction rate at the positively curved locations

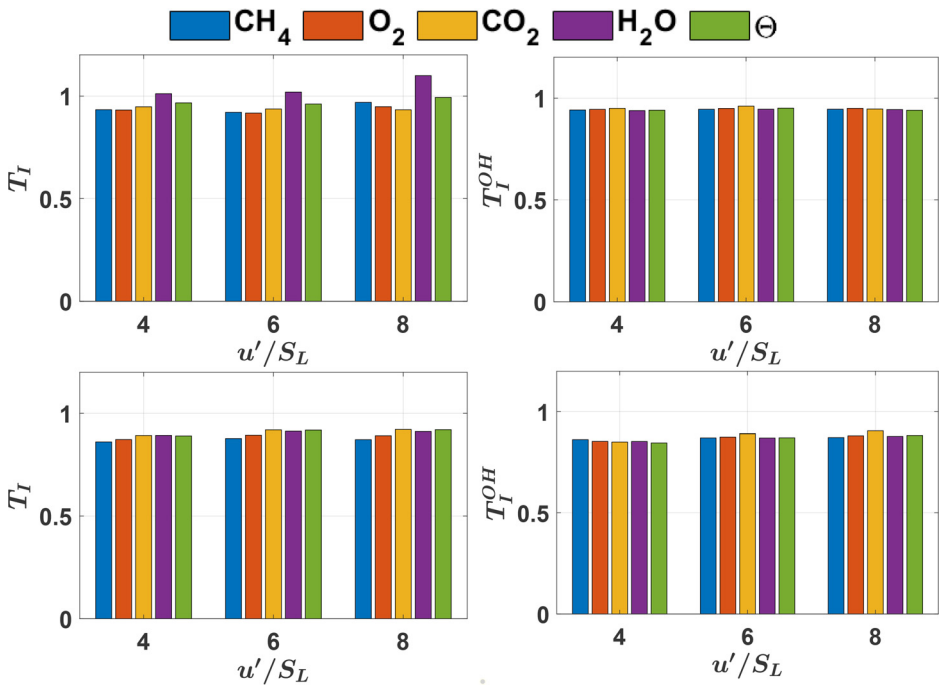

FIG. 10. Values of $T_I = \Omega/S$ (first column) and $T_I^{OH} = \Omega/S^{OH}$ (second column) for c definitions based on CH_4, O_2, CO_2, and H_2O mass fractions and non-dimensional temperature Θ for different initial values of u'/S_L for $\phi = 0.8$ and 1.0 (first to second row) at the time when statistics were extracted (i.e., at $1.0\delta_{th}/S_L$ for $\phi = 0.8$, which corresponds to $1.9\delta_{th}/S_L$ for $\phi = 1.0$).

tend to oppose the effects induced by the reduced $\dot{w}_c$ values at the negatively curved locations for CO_2 mass fraction-based reaction progress variable. Therefore, Ω values remain comparable for a given set of values of initial turbulence intensity and equivalence ratio (see Fig. 4). However, the extent of wrinkling of c isosurfaces is different for different definitions of c for a given initial turbulence intensity (see Fig. 4) due to the combination of differential diffusion effects and their different spatial locations, which leads to differences in S values. Thus, the relative magnitudes of Ω and S determine the magnitude of T_I and yield a value smaller than unity indicating $\langle \rho S_d \rangle_V = \int_V \dot{w}_c dV / \int_V |\nabla c| dV$ being smaller than its laminar value (i.e., $\rho_0 S_L$) for CH_4, O_2, and CO_2 mass fraction-based reaction progress variables irrespective of the value of u'/S_L.

The smaller extent of flame wrinkling for H_2O mass fraction-based c isosurfaces in comparison with the wrinkling of c isosurfaces based on alternative definitions of reaction progress variable has been shown in the context of Fig. 4 and discussed in detail by Keil *et al.*[47] for the $\phi = 1.0$ case, and the same phenomenon is observed for $\phi = 0.8$. This leads to higher values of $T_1 = \Omega/S = \langle \rho S_d \rangle_V / \rho_0 S_L$ in the case of H_2O mass fraction-based reaction progress variable than the corresponding values for CH_4, O_2, and CO_2 mass fraction-based reaction progress variables (see Fig. 10).

From the foregoing, it is evident that Eq. (2), at least when interpreted as a strict equality, may not strictly hold even for statistically planar flames, which have the global effective Lewis number Le_{eff} close to unity. It was discussed elsewhere[9,28] that a modified flame speed $S_L{}'$ can be defined as follows: $S_L{}' = \langle \rho S_d \rangle_V / \rho_0$, which leads to an exact equality between $S_T/S_L{}'$ and A_T/A_L. However, the magnitudes of T_I and T_I^{OH} remain of the order of unity suggesting that Eq. (2) holds in an order of magnitude sense (i.e., $S_T/S_L \sim A_T/A_L$) for the cases considered here.

It is worth noting that the turbulent burning velocity can be expressed as follows:

$$\rho_0 A_L S_T = \int_V \dot{w} dV = \int_V \rho S_d |\nabla c| dV = \int_V \overline{(\rho S_d)}_s \Sigma_{\text{gen}} dV, \quad (6)$$

where $\Sigma_{\text{gen}} = \overline{|\nabla c|}$ is the generalized flame surface density (FSD)[37] and $\overline{(\rho S_d)}_s = \overline{\rho S_d |\nabla c|} / \Sigma_{\text{gen}}$ is the surface-weighted value of $\rho S_d = \rho (Dc/Dt)/|\nabla c|$[37,39] with the overbar suggesting a Reynolds averaging/large eddy simulation (LES) filtering operation, as appropriate. The quantity $\overline{(\rho S_d)}_s$ can be expressed as follows: $\overline{(\rho S_d)}_s = I_0 \rho_0 S_L$ where I_0 depends on the flame stretch.[23] Using $\overline{(\rho S_d)}_s = I_0 \rho_0 S_L$ in $\int_V \overline{(\rho S_d)}_s \Sigma_{\text{gen}} dV$ yields $\rho_0 A_L S_T = \rho_0 A_T S_L'$ or $S_T/S_L' = A_T/A_L$ where $S_L' = S_L \int_V I_0 \Sigma_{\text{gen}} dV / \int_V \Sigma_{\text{gen}} dV = \int_V \rho S_d |\nabla c| dV / \rho_0 \int_V |\nabla c| dV = \langle \rho S_d \rangle_V / \rho_0$ is the stretch-corrected flame speed. It was demonstrated in Ref. 9 that the expression $S_T/S_L' = A_T/A_L$ remains valid irrespective of the characteristic Lewis number but S_L' is a quantity, which needs to be modeled, and it is extremely difficult to estimate S_L' by experimental means. Therefore, it is not straightforward to apply Eq. (6) for general premixed flame configurations.

IV. ANALYSIS OF DAMKÖHLER'S SECOND HYPOTHESIS

The normalized flame surface area A_T/A_L can be expressed as $A_T/A_L = (\eta_0/\eta_i)^{D_f - 2}$,[57] where D_f is the fractal dimension, η_0 is the outer cutoff scale, and η_i is the inner cutoff scale. It was argued in previous analyses[12,58,59] that for $Da < 1$ and $Ka > 1$, the inner cutoff scale η_i can be taken to scale with the Obukhov–Corrsin scale $\eta_{OC} = Sc^{-3/4} \eta$ (i.e., $\eta_i \sim \eta_{OC}$) where η is the Kolmogorov length scale. For gaseous flows, the Schmidt number remains of the order of unity (i.e., $Sc \sim O(1)$)[59] and thus η_i can in turn be scaled with respect to η (i.e., $\eta_i \sim \eta$). In the context of Reynolds-averaged Navier–Stokes (RANS) simulations, η_0 can be taken to scale with the integral length scale l (i.e., $\eta_0 \sim l$). Equating the right-hand sides of Eqs. (2) and (3) leads to $\sqrt{D_t/D} \sim \sqrt{u' l/D} \sim \sqrt{Re_t} = (\eta_0/\eta_i)^{D_f - 2} \sim (l/\eta)^{D_f - 2} \sim (Re_t^{3/4})^{D_f - 2}$ where $Re_t = \rho_0 u' l/\mu_0$ is the turbulent Reynolds number. The expression $\sqrt{Re_t} \sim (Re_t^{3/4})^{D_f - 2}$ suggests that one obtains $D_f = 8/3$ for simultaneous validity of Eqs. (2) and (3) in an order of magnitude sense where, D_f and η_i are evaluated in the following manner:[22,58,60,61]

$$\log \Xi_v = \log \left[\int_V \Sigma_{gen} dV \Big/ \int_V \Sigma_{res} dV \right] = (D_f - 2)[\log(\Delta/\delta_{th}) + \log(\delta_{th}/\eta_i)]. \quad (7)$$

Here, $\Sigma_{gen} = \widetilde{|\nabla c|}$ is the generalized FSD in the context of LES[37] and $\Sigma_{res} = |\nabla \tilde{c}|$ is the resolved FSD, where $\tilde{q}$ denotes the LES filtered value of a general quantity q and Δ is the LES filter width. A linear profile of the variation of $\log \Xi_v$ with $\log(\Delta/\delta_{th})$ is indicative of $A_T/A_L = (\eta_0/\eta_i)^{D_f - 2}$. Such a linear behavior has been obtained for $\Delta > \delta_{th}$ in several previous analyses,[58,60,61] and a qualitatively similar behavior has been observed here (not shown here for brevity). The filter size for which $\log \Xi_v$ vanishes according to the power-law $\Xi_v = (\Delta/\eta_i)^{D_f - 2}$ provides the inner cutoff scale η_i. The slope of the linear part of $\log \Xi_v$ variation with $\log(\Delta/\delta_{th})$ yields the value of $(D_f - 2)$ and thus provides the measure of the fractal dimension D_f. It can be seen from Table II that D_f remains smaller than 8/3 but close to 7/3 and η_i ranges between $7.0\eta - 16.0\eta$ for all cases considered here for CH_4 mass fraction-based reaction progress variable (results are qualitatively similar for other c definitions), which is consistent with previous experimental[15,45] and computational[58,60,62] analyses. These values are different from the assumptions $D_f = 8/3$ and $\eta_i \sim \eta$, which were made for the simultaneous validity of Damköhler's hypotheses [i.e., $\sqrt{D_t/D} \sim \sqrt{u' l/D} \sim \sqrt{Re_t} = (\eta_0/\eta_i)^{D_f - 2} \sim (l/\eta)^{D_f - 2} \sim (Re_t^{3/4})^{D_f - 2}$]. Thus, Damköhler's first and second hypotheses do not remain simultaneously valid for the cases considered here. It is worth noting that under the decaying turbulence, the Damköhler number at the end of simulation in this work assumes values of the order of unity, whereas Damköhler's second hypothesis is strictly valid for $Da < 1$. Moreover, a recent analysis by Sabelnikov and Lipatnikov[59] indicated that

TABLE II. Values of D_f and η_i/η for all cases considered here for CH_4 mass fraction-based reaction progress variable.

	$\phi = 0.8$		$\phi = 1.0$	
Initial u'/S_L	D_f	η_i/η	D_f	η_i/η
4.0	2.24	7.71	2.20	10.84
6.0	2.27	10.78	2.21	14.81
8.0	2.34	13.13	2.21	16.47

premixed flames can potentially exhibit bifractal nature and the asymptotic value of $D_f = 8/3$ is obtained only for $l \ll \delta_{th} Ka$, whereas an asymptotic value of $D_f = 7/3$ is obtained only for $l > \delta_{th} Ka$. It can be seen from Table I that $l \ll \delta_{th} Ka$ is not realized in the cases considered here and thus $D_f = 8/3$ may not be realized for this database, which also indicates that the simultaneous validity of Damköhler's hypotheses cannot be expected for this database. As Fig. 10 suggests that the exact equality between S_T/S_L and A_T/A_L does not hold for the cases considered here, the prediction of Damköhler's second hypothesis [i.e., Eq. (3)] will be analyzed next in this paper in order to assess the extent of its departure from S_T/S_L extracted from DNS data in the thin reaction zone regime (i.e., $Ka > 1$) flames considered here. Despite the range of parameters for which the validity of Eq. (3) will be analyzed, being limited, it remains comparable to that used in previous DNS studies by other research groups.[8,18] Moreover, Eq. (3) is strictly valid for $l/\delta_{th} < 1$ but this length scale separation has limited practical relevance[2,20,21] and this expression [i.e., Eq. (3)] was used previously for premixed combustion modeling in the thin reaction zone regime,[12] so there is some merit assessing the second hypothesis by Damköhler, even for limited parameters, in the thin reaction zone regime because a valid concept is expected to work well also for a limited range of parameters.

The turbulent diffusivity D_t at the leading edge of a statistically planar turbulent premixed flame brush can be estimated as follows: $D_t = [-\overline{\rho u_1'' c''}/\{\overline{\rho}(\partial \tilde{c}/\partial x_1)\}]_{LE}$ where the overbar and tilde refer to Reynolds-averaged and Favre-averaged values with the double prime indicating Favre fluctuations. The subscript "LE" refers to the value at the leading edge of the turbulent flame brush, which can be characterized by $\bar{c} = \epsilon$ where ϵ is a predetermined small number. This yields the following expression according to Damköhler's second hypothesis:[18]

$$(S_T/S_L) = \sqrt{[-\overline{\rho u_1'' c''}/\{\overline{\rho} D(\partial \tilde{c}/\partial x_1)\}]_{LE}}. \tag{8}$$

The leading edge is chosen for this analysis because a gradient-type transport (thus a positive value of D_t) is realized at the leading edge even when a counter-gradient-type transport is obtained within the flame brush[22–24] and thus Eq. (3) can safely be applied at the leading edge of the flame brush. A similar argument is used for justifying the validity of the results of Kolmogorov–Petrovskii–Piskunov (KPP) theorem at the leading edge of the flame brush in the event of counter-gradient transport.[23]

Alternatively, D_t is often modeled as follows:[18] $D_t = \nu_t/Sc_t = C_\mu \tilde{k}^2/(Sc_t \tilde{\varepsilon})$ where ν_t is the eddy kinematic viscosity, Sc_t is the turbulent Schmidt number, and $C_\mu = 0.09$ is a model parameter with $\tilde{k} = \overline{\rho u_i'' u_i''}/2\overline{\rho}$ and $\tilde{\varepsilon} = \overline{\mu(\partial u_i''/\partial x_j)(\partial u_i''/\partial x_j)}/\overline{\rho}$ being the turbulent kinetic energy and its dissipation rate, respectively. The approximation $D_t = \nu_t/Sc_t = C_\mu \tilde{k}^2/(Sc_t \tilde{\varepsilon})$ has well-known limitations, but this expression is often used in the context of RANS simulations and therefore it is useful to assess the implications of using this estimation of D_t in the context of Damköhler's second hypothesis.

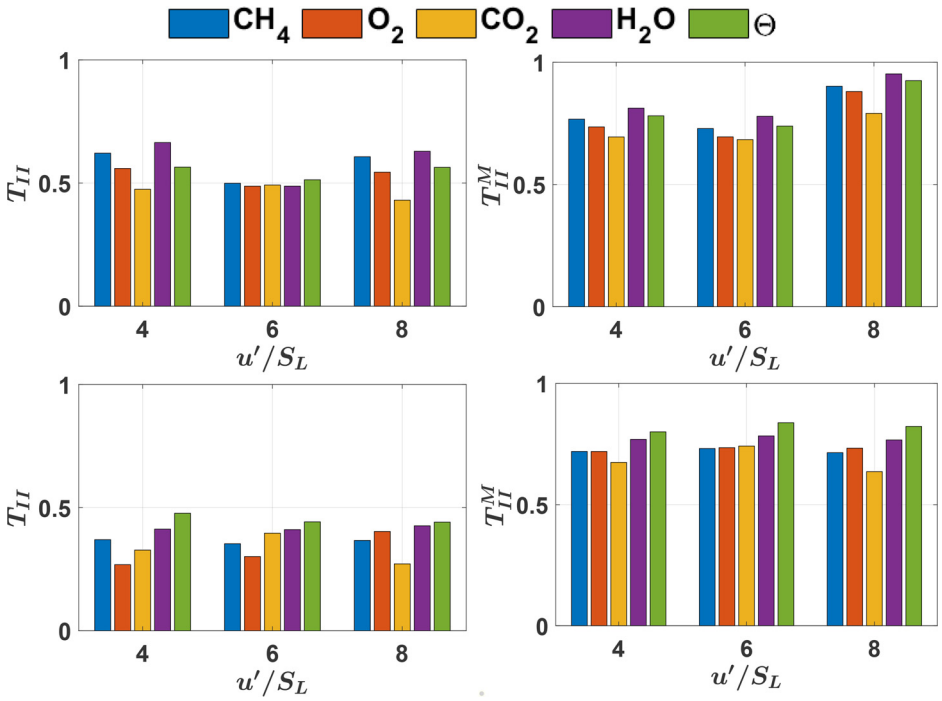

FIG. 11. Values of $T_{II} = (S_T/S_L)/\sqrt{[-\overline{\rho u_1'' c''}/\{\overline{\rho} D(\partial \tilde{c}/\partial x_1)\}]_{LE}}$ (first column) and $T_{II}^M = (S_T/S_L)/\sqrt{(C_\mu Sc/Sc_t)[\overline{\rho}\,\tilde{k}^2/\mu\tilde{\varepsilon}]_{LE}}$ (second column) for c definitions based on CH_4, O_2, CO_2, and H_2O mass fractions and non-dimensional temperature Θ for different initial values of u'/S_L for $\phi = 0.8$ and 1.0 (first to second row) at the time when statistics were extracted (i.e., at $1.0\delta_{th}/S_L$ for $\phi = 0.8$, which corresponds to $1.9\delta_{th}/S_L$ for $\phi = 1.0$).

This yields the following expression according to Damköhler's second hypothesis:[22]

$$S_T/S_L = \sqrt{(C_\mu Sc/Sc_t)[\overline{\rho}\,\tilde{k}^2/\mu\tilde{\varepsilon}]_{LE}}, \quad (9)$$

where $Sc = \mu/(\rho D)$ is the molecular Schmidt number and Sc_t remains of the order of unity (i.e., $Sc_t \sim 1.0$). The predictions of $T_{II} = (S_T/S_L)/\sqrt{\left[-\overline{\rho u_1'' c''}/\{\overline{\rho} D(\partial\tilde{c}/\partial x_1)\}\right]_{LE}}$ and $T_{II}^M = (S_T/S_L)/\sqrt{(C_\mu Sc/Sc_t)\left[\overline{\rho}\,\tilde{k}^2/\mu\tilde{\varepsilon}\right]_{LE}}$ according to Eqs. (8) and (9), respectively, are shown in Fig. 11 exemplarily for the leading edge defined by $\overline{c} = 0.005$ where the molecular diffusivity D at the leading edge is evaluated for c definitions based on CH_4, O_2, CO_2, and H_2O mass fractions. The reaction progress diffusivity D is estimated as $D = (1 - Y_k)/\sum_{j\neq k} X_j/D_{jk}$, where X_j is the mole fraction of species j, D_{jk} is the binary diffusion coefficient, and species k is used to define the reaction progress variable. Qualitatively similar results, as that of the mass fraction-based reaction progress variable, are obtained when the non-dimensional temperature Θ is used as the reaction progress variable c and thermal diffusivity is used for D (see Fig. 11).

Figure 11 shows that both T_{II} and T_{II}^M remain smaller than unity for all cases, but the magnitudes of T_{II} and T_{II}^M indicate that Eqs. (8) and (9) remain valid in an order of magnitude sense rather in equality (i.e., $S_T/S_L \sim \sqrt{[-\overline{\rho u_1'' c''}/\{\overline{\rho} D(\partial\tilde{c}/\partial x_1)\}]_{LE}}$ and $S_T/S_L \sim \sqrt{(C_\mu Sc/Sc_t)[\overline{\rho}\,\tilde{k}^2/\mu\tilde{\varepsilon}]_{LE}}$). However, the deviation of T_{II} from unity could be up to 70% (e.g., O_2 mass fraction-based reaction progress variable for $\phi = 1.0$). These findings are also qualitatively consistent with previous experimental findings by Osborne *et al.*[27] These findings remain qualitatively valid within the range $\overline{c} = 0.001$–0.005 (not shown here) and are consistent with previous analysis,[22] which showed based on the equilibrium of strain rate and curvature contributions of the FSD transport equation for $Ka \gg 1$ that $S_T/S_L \sim \sqrt{\Gamma(D_t/D)}$ where $\Gamma = f(u'/S_L, l/\delta_{th})$ is the efficiency function.[63] Nivarti *et al.*[21] suggested an alternative empirical relation $S_T/S_L = (A_T/A_L)\sqrt{D_t/D}$. However, it can be seen from both Figs. 10 and 11 that T_I, T_I^{OH}, T_{II}, and T_{II}^M assume values smaller than unity suggesting that both A_T/A_L and $\sqrt{D_t/D}$ remain greater than S_T/S_L for all choices of c for $\phi = 1.0$ cases. This is also valid for the $\phi = 0.8$ cases for reaction progress variable definitions based on CH_4, O_2, CO_2 mass fractions. Although T_I remains greater than unity for initial $u'/S_L = 8.0$ in the case of $\phi = 0.8$ for H_2O mass fraction based reaction progress variable, the higher values of $\sqrt{D_t/D}$ compared to S_T/S_L overcome (A_T/A_L) being smaller than S_T/S_L. Thus, $(A_T/A_L)\sqrt{D_t/D}$ significantly overpredicts S_T/S_L for all cases considered here, and for this reason, the performance of $S_T/S_L = (A_T/A_L)\sqrt{D_t/D}$ is not explicitly shown here. Figures 10 and 11 further illustrate that Damköhler's hypotheses [see Eqs. (2) and (3)] in their original forms should be considered only in an order of magnitude sense for the parameter range investigated in this work, instead of considering the equality between S_T/S_L and A_T/A_L and between S_T/S_L and $\sqrt{D_t/D}$ even for the thin reaction zone regime flames with global effective Lewis number $Le_{eff} \approx 1.0$.

V. CONCLUSIONS

The effects of the definition of the reaction progress variable and equivalence ratio on the validity of Damköhler's hypotheses in the thin reaction zone regime are assessed by considering multi-step chemistry DNS data of statistically planar CH_4–air flames with $\phi = 0.8$ and 1.0. The global effective Lewis number remains close to unity for these equivalence ratios for methane–air flames. An inequality between S_T/S_L and A_T/A_L is obtained for all cases, but the ratios of S_T/S_L and A_T/A_L remain of the order of unity. The local differential diffusion effects contribute to the lack of equality between S_T/S_L and A_T/A_L. Moreover, S_T/S_L has been found to be smaller than that of $\sqrt{D_t/D}$ for both $\phi = 0.8$ and 1.0 irrespective of the definition of reaction progress variable when both D_t and D are evaluated at the leading edge of the flame brush. The findings of the current analysis suggest that Damköhler's first and second hypotheses should only be considered valid in an order of magnitude sense instead of an equality between S_T/S_L and A_T/A_L (maximum deviation is 14% for the cases considered here) and between S_T/S_L and $\sqrt{D_t/D}$ (maximum deviation is 70% for the cases considered here) in the thin reaction zone regime even for statistically planar premixed turbulent flames with global effective Lewis numbers close to unity. It is worth noting that several experimental analyses[15–17] reported larger discrepancy between S_T/S_L and A_T/A_L than what is reported in this and recent DNS[9,14] analyses. It was discussed elsewhere[9,54] that the discrepancy between S_T/S_L and A_T/A_L is augmented in the configurations where a considerable mean flame curvature exists, and therefore, further analyses will be needed in setups where the flame has a non-zero mean curvature. Finally, it is worth noting that the validity of Damköhler's hypotheses has been assessed here for a limited parameter range within the thin reaction zone regime, so further analyses will be necessary for a broader range of parameters, which will form the basis of future investigations.

ACKNOWLEDGMENTS

The authors are grateful to the Engineering and Physical Sciences Research Council (Nos. EP/R026369/1 and EP/S0254154/1) for financial and computational support and the high-performance computing (HPC) facility at Newcastle University (ROCKET).

AUTHOR DECLARATIONS

Conflict of Interest

The authors have no conflicts to disclose.

DATA AVAILABILITY

The data that support the findings of this study are available from the corresponding author upon reasonable request.

APPENDIX: RELEVANT STATISTICS HALFWAY THROUGH THE SIMULATION

The statistics presented in Figs. 4, 6, 10, and 11 remain qualitatively similar halfway through the simulation, which is demonstrated in Figs. 12–15, respectively, in this appendix. A comparison between Figs. 4, 6, 10, and 11 with Figs. 12–15 reveals that all the conclusions drawn from Figs. 4, 6, 10, and 11 do not change since the midway through the simulation time for the cases considered here.

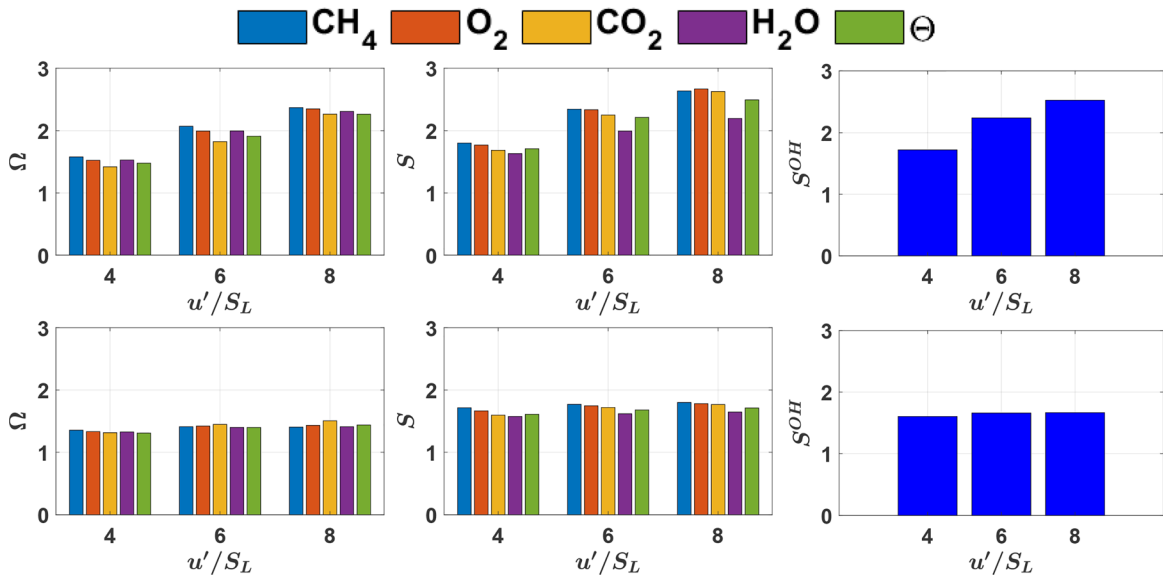

FIG. 12. Values of $\Omega = \int_V \dot{w}_c dV / \left[\int_V \dot{w}_c dV\right]_L$, $S = \int_V |\nabla c| dV / \left[\int_V |\nabla c| dV\right]_L$, and $S^{OH} = A_T^{OH}/A_L$ for c definitions based on CH_4, O_2, CO_2, and H_2O mass fractions and non-dimensional temperature Θ for different initial values of u'/S_L for both $\phi = 0.8$ and 1.0 (first to second row) halfway through the simulation (i.e., at $0.5\delta_{th}/S_L$ for $\phi = 0.8$, which corresponds to $1.0\delta_{th}/S_L$ for $\phi = 1.0$).

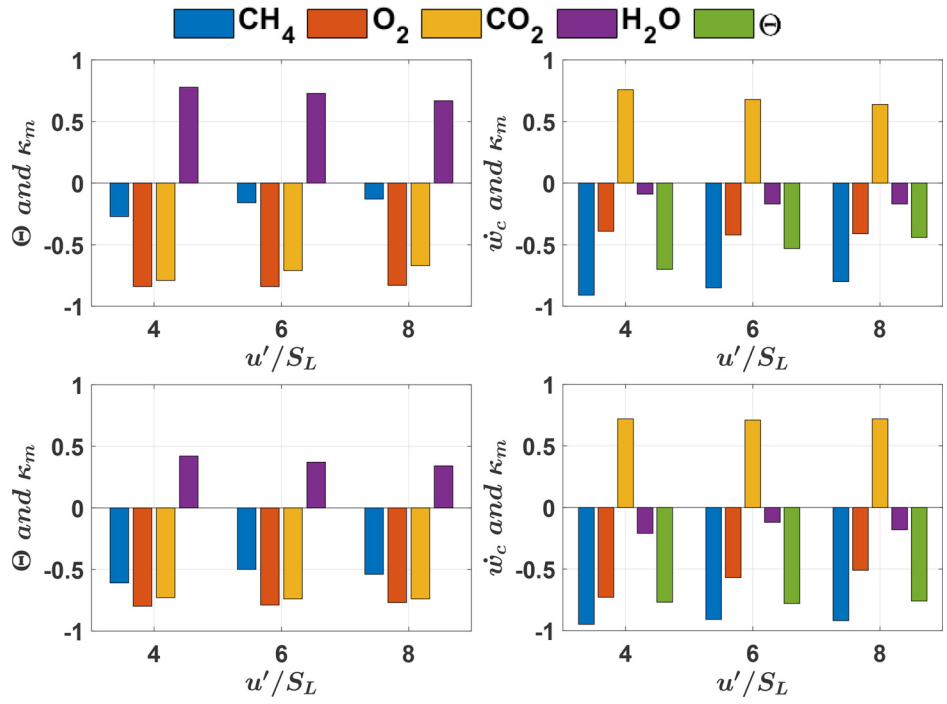

FIG. 13. Correlation coefficients between Θ and κ_m for $c = 0.8$ isosurface based on CH_4, O_2, CO_2, and H_2O mass fractions (first column) and correlation coefficients between $\dot{w}_c$ and κ_m for $c = 0.8$ isosurface based on CH_4, O_2, CO_2, and H_2O mass fractions and non-dimensional temperature Θ (for which $\dot{w}_c = \dot{w}_\Theta$ is considered) (second column) for different initial values of u'/S_L for both $\phi = 0.8$ and 1.0 (first to second row) halfway through the simulation (i.e., at $0.5\delta_{th}/S_L$ for $\phi = 0.8$, which corresponds to $1.0\delta_{th}/S_L$ for $\phi = 1.0$).

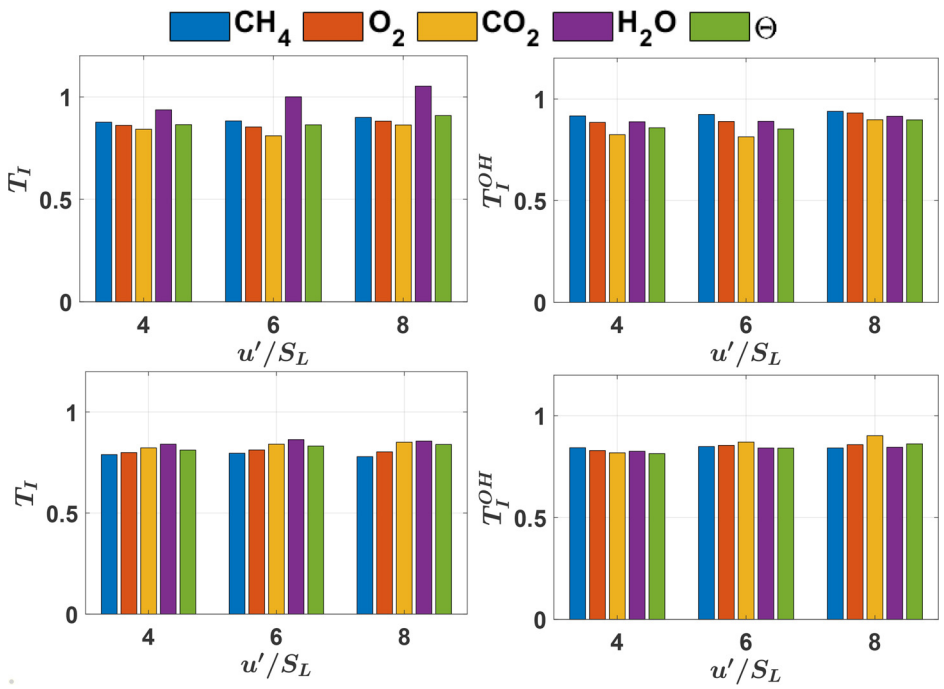

FIG. 14. Values of $T_I = \Omega/S$ (first column) and $T_I^{OH} = \Omega/S^{OH}$ (second column) for c definitions based on CH_4, O_2, CO_2, and H_2O mass fractions and non-dimensional temperature Θ for different initial values of u'/S_L for $\phi = 0.8$ and 1.0 (first to second row) halfway through the simulation (i.e., at $0.5\delta_{th}/S_L$ for $\phi = 0.8$, which corresponds to $1.0\delta_{th}/S_L$ for $\phi = 1.0$).

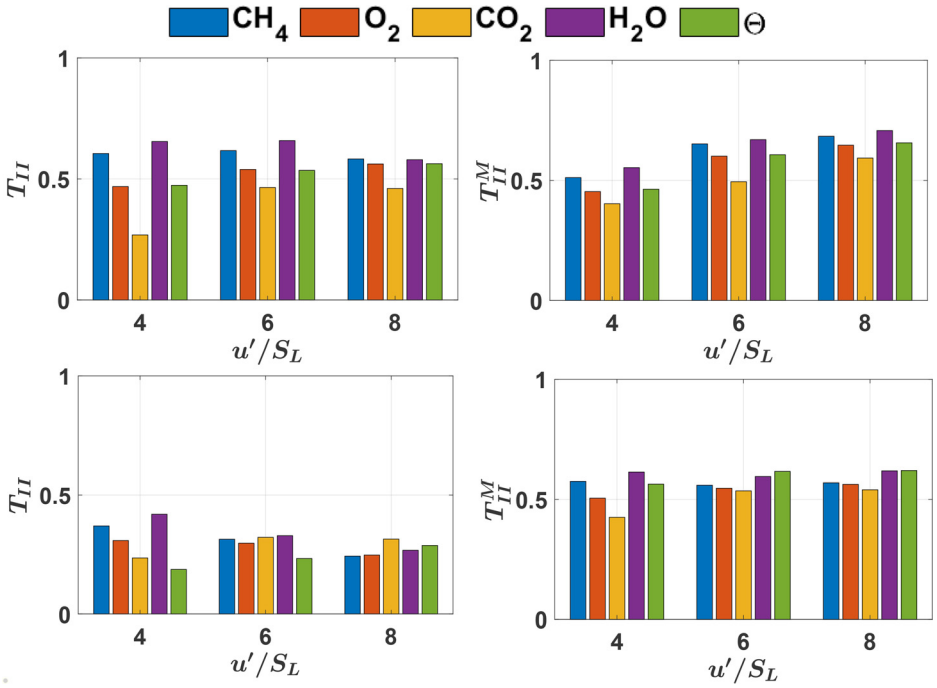

FIG. 15. Values of $T_{II} = (S_T/S_L)/\sqrt{[-\overline{\rho u_i'' c''}/\{\overline{\rho} D(\partial\tilde{c}/\partial x_1)\}]_{LE}}$ (first column) and $T_{II}^{M} = (S_T/S_L)/\sqrt{(C_\mu Sc/Sc_t)[\overline{\rho}\,\tilde{k}^2/\mu\tilde{\varepsilon}]_{LE}}$ (second column) for c definitions based on CH_4, O_2, CO_2, and H_2O mass fractions and non-dimensional temperature Θ for different initial values of u'/S_L for $\phi = 0.8$ and 1.0 (first to second row) halfway through the simulation (i.e., at $0.5\delta_{th}/S_L$ for $\phi = 0.8$, which corresponds to $1.0\delta_{th}/S_L$ for $\phi = 1.0$).

REFERENCES

[1]G. Damköhler, Der Einfluss der Turbulenz auf die Flammengeschwindigkeit in Gasgemischen, Z. Elektrochem. Angew. Phys. Chem. **46**, 601–626 (1940).
[2]J. F. Driscoll, "Turbulent premixed combustion: Flamelet structure and its effect on turbulent burning velocities," Prog. Energy Combust Sci. **34**, 91–134 (2008).
[3]T. J. Poinsot and D. Veynante, *Theoretical and Numerical Combustion*, 1st ed. (R.T. Edwards, 2001).
[4]X. Wang, X. Cheng, H. Lu, Y. Xu, Y. Liu, R. Wang, and J. Yao, "Quantifying the role of Darrieus–Landau instability in turbulent premixed flame speed determination at various burner sizes," Phys. Fluids **33**, 025104 (2021).
[5]M. Bambauer, N. Chakraborty, M. Klein, and J. Hasslberger, "Vortex dynamics and fractal structures in reactive and nonreactive Richtmyer–Meshkov instability," Phys. Fluids **33**, 044114 (2021).
[6]R. Rasool, M. Klein, and N. Chakraborty, "Flame surface density based mean reaction rate closure for Reynolds averaged Navier Stokes methodology in turbulent premixed Bunsen flames with non-unity Lewis number," Combust. Flame **239**, 111766 (2021).
[7]A. N. Lipatnikov, V. A. Sabelnikov, S. Nishiki, and T. Hasegawa, "Letter: Does flame-generated vorticity increase turbulent burning velocity?," Phys. Fluids **30**, 081702 (2018).
[8]G. V. Nivarti and R. S. Cant, "Direct numerical simulation of the bending effect in turbulent premixed flames," Proc. Combust. Inst. **36**, 1903–1910 (2017).
[9]N. Chakraborty, D. Alwazzan, M. Klein, and R. S. Cant, "On the validity of Damköhler's first hypothesis in turbulent Bunsen burner flames: A computational analysis," Proc. Combust. Inst. **37**, 2231–2239 (2019).
[10]U. Ahmed, N. Chakraborty, and M. Klein, "Insights into the bending effect in premixed turbulent combustion using the flame surface density transport," Combust. Sci. Technol. **191**, 898–920 (2019).
[11]A. Varma, U. Ahmed, N. Chakraborty, and M. Klein, "Effects of turbulent length scale on the bending effect of turbulent burning velocity in premixed turbulent combustion," Combust. Flame **233**, 111569 (2021).
[12]N. Peters, *Turbulent Combustion*, 1st ed. (Cambridge University Press, 2000).
[13]A. J. Aspden, M. S. Day, and J. B. Bell, "Turbulence–flame interactions in lean premixed hydrogen: Transition to the distributed burning regime," J. Fluid Mech. **680**, 287–320 (2011).
[14]A. Attili, S. Luca, D. Denker, F. Bisetti, and H. Pitsch, "Turbulent flame speed and reaction layer thickening in premixed jet flames at constant Karlovitz and increasing Reynolds numbers," Proc. Combust. Inst. **38**, 2939–2947 (2021).
[15]F. T. C. Yuen and O. L. Gulder, "Dynamics of lean-premixed turbulent combustion at high turbulence intensity," Combust. Sci. Technol. **182**, 544–558 (2010).
[16]Z. Wang, B. Zhou, S. Yu, C. Brackmann, Z. Li, M. Richter, M. Alden, and X.-S. Bai, "Structure and burning velocity of turbulent premixed methane/air jet flames in thin-reaction zones and distributed reaction zones regimes," Proc. Combust. Inst. **37**, 2537–2544 (2019).
[17]J. F. Driscoll, J. H. Chen, A. W. Skiba, C. D. Carter, E. R. Hawkes, and H. Wang, "Premixed flames subjected to extreme turbulence: Some questions and recent answers," Prog. Energy Combust. Sci. **76**, 100802 (2020).
[18]J. Daou, J. Dold, and M. Matalon, "The thick flame asymptotic limit and Damköhler's hypothesis," Combust. Theory Modell. **6**, 141–153 (2002).
[19]G. V. Nivarti and R. S. Cant, "Scalar transport and the validity of Damköhler's hypotheses for flame propagation in intense turbulence," Phys. Fluids **29**, 085107 (2017).
[20]Ö. Gulder, "Contribution of small scale turbulence to burning velocity of flamelets in the thin reaction zone regime," Proc. Combust. Inst. **31**, 1369–1375 (2007).
[21]G. V. Nivarti, R. S. Cant, and S. Hochgreb, "Reconciling turbulent burning velocity with flame surface area in small-scale turbulence," J. Fluid Mech. **858**, R1 (2019).
[22]U. Ahmed, A. Herbert, N. Chakraborty, and M. Klein, "On the validity of Damköhler's second hypothesis in statistically planar turbulent premixed flames in the thin reaction zones regime," Proc. Combust. Inst. **38**, 3039–3047 (2021).
[23]K. N. C. Bray, "Studies of the turbulent burning velocity," Proc. R. Soc. London, Ser. A **431**, 315–335 (1990).
[24]N. Chakraborty and R. S. Cant, "Effects of Lewis number on scalar transport in turbulent premixed flames," Phys. Fluids **21**, 035110 (2009).
[25]H. Wenzel and N. Peters, "Direct numerical simulation and modeling of kinematic restoration, dissipation and gas expansion effects of premixed flames in homogeneous turbulence," Combust. Sci. Technol. **158**, 273–297 (2000).
[26]V. A. Sabelnikov, R. Yu, and A. N. Lipatnikov, "Thin reaction zones in constant-density turbulent flows at low Damköhler numbers: Theory and simulations," Phys. Fluids **31**, 055104 (2019).
[27]J. R. Osborne, S. A. Ramji, C. D. Carter, and A. D. Steinberg, "Relationship between local reaction rate and flame structure in turbulent premixed flames from simultaneous 10 kHz TPIV, OH PLIF and CH_2O PLIF," Proc. Combust. Inst. **36**, 1835–1841 (2017).
[28]M. Klein, A. Herbert, H. Kosaka, B. Böhm, A. Dreizler, N. Chakraborty, V. Papapostolou, H. G. Im, and J. Hasslberger, "Evaluation of flame area based on detailed chemistry DNS of premixed turbulent hydrogen-air flames in different regimes of combustion," Flow, Turbul. Combust. **104**, 403–419 (2020).
[29]N. Chakraborty and R. S. Cant, "Influence of Lewis number on curvature effects in turbulent premixed flame propagation in the thin reaction zones regime," Phys. Fluids **17**, 105105 (2005).
[30]N. Chakraborty and R. S. Cant, "Effects of Lewis number on flame surface density transport in turbulent premixed combustion," Combust. Flame **158**, 1768–1787 (2011).
[31]J. K. Bechtold and M. Matalon, "The dependence of the Markstein length on stoichiometry," Combust. Flame **127**, 1906–1913 (2001).
[32]E. F. Tarrazo, L. S. Antonio, A. Liñán, and F. A. Williams, "A simple one-step chemistry model for partially premixed hydrocarbon combustion," Combust. Flame **147**, 32–38 (2006).
[33]R. S. Cant, *SENGA2 Manual, CUED-THERMO-2012/04*, 2nd ed. (Cambridge University, Cambridge, 2012).
[34]M. D. Smooke and V. Giovangigli, "Premixed and nonpremixed test flame results," in *Reduced Kinetic Mechanisms and Asymptotic Approximations for Methane-Air Flames* (Springer, Berlin, 1991), pp. 29–47.
[35]T. Poinsot and S. K. Lele, "Boundary conditions for direct simulation of compressible viscous flows," J. Comput. Phys. **101**, 104–129 (1992).
[36]R. S. Rogallo, "Numerical experiments in homogeneous turbulence," NASA Technical Memorandum No. 81315 (NASA Ames Research Center, California, 1981).
[37]M. Boger, D. Veynante, H. Boughanem, and A. Trouvé, "Direct numerical simulation analysis of flame surface density concept for large eddy simulation of turbulent premixed combustion," Proc. Combust. Inst. **27**, 917–925 (1998).
[38]H. Reddy and J. Abraham, "Two-dimensional direct numerical simulation evaluation of the flame surface density model for flames developing from an ignition kernel in lean methane/air mixtures under engine conditions," Phys. Fluids **24**, 105108 (2012).
[39]A. Trouvé and T. J. Poinsot, "The evolution equation for flame surface density in turbulent premixed combustion," J. Fluid Mech. **278**, 1–32 (1994).
[40]S. Zhang and C. J. Rutland, "Premixed flame effects on turbulence and pressure related terms," Combust. Flame **102**, 447–461 (1995).
[41]P. H. Paul and H. Najm, "Planar laser-induced fluorescence imaging of flame heat release rate," Proc. Combust. Inst. **27**, 43–50 (1998).
[42]R. Balachandran, B. O. Ayoola, C. F. Kaminski, A. P. Dowling, and E. Mastorakos, "Planar laser-induced fluorescence imaging of flame heat release rate," Combust. Flame **143**, 37–55 (2005).
[43]A. Faryoux, K. Zähringer, O. Gicquel, and J. C. Rolon, "Experimental and numerical determination of heat release in counterflow premixed laminar flames," Proc. Combust. Inst. **30**, 251–257 (2005).
[44]T. M. Wabel, A. W. Skiba, J. E. Temme, and J. F. Driscoll, "Measurements to determine the regimes of premixed flames in extreme turbulence," Proc. Combust. Inst. **36**, 1809–1816 (2017).
[45]A. W. Skiba, C. D. Carter, S. D. Hammack, and J. F. Driscoll, "High-fidelity flame-front wrinkling measurements derived from fractal analysis of turbulent premixed flames with large Reynolds numbers," Proc. Combust. Inst. **38**, 2809–2816 (2021).
[46]Y. Minamoto and N. Swaminathan, "Scalar gradient behaviour in MILD combustion," Combust. Flame **161**, 1063–1075 (2014).
[47]F. B. Keil, M. Amzehnhoff, U. Ahmed, N. Chakraborty, and M. Klein, "Comparison of flame propagation statistics extracted from DNS based on simple and detailed chemistry part 2: Influence of choice of reaction progress variable," Energies **14**, 5695 (2021).

[48]Y.-C. Chen and M. S. Mansour, "Topology of turbulent premixed flame fronts resolved by simultaneous planar imaging of LIPF of OH radical and Rayleigh scattering," Exp. Fluids **26**, 277–287 (1999).
[49]A. W. Skiba, C. D. Carter, S. D. Hammack, and J. F. Driscoll, "Premixed flames subjected to extreme levels of turbulence part II: Surface characteristics and scalar dissipation rates," Combust. Flame (Published online 2021), p. 111703.
[50]C. J. Rutland and A. Trouve, "Direct Simulations of premixed turbulent flames with nonunity Lewis numbers," Combust. Flame **94**, 41–57 (1993).
[51]P. Clavin and F. A. Williams, "Effects of molecular diffusion and thermal expansion on the structure and dynamics of turbulent premixed flames in turbulent flows of large scale and small intensity," J. Fluid Mech. **116**, 251–282 (1982).
[52]P. Pelce and P. Clavin, "Influence of hydrodynamics and diffusion upon the stability limits of laminar premixed flames," J. Fluid Mech. **124**, 219–237 (1982).
[53]F. Dinkelacker, B. Manickam, and S. P. R. Muppala, "Modelling and simulation of lean premixed turbulent methane/hydrogen/air flames with an effective Lewis number approach," Combust. Flame **158**, 1742–1749 (2011).
[54]G. Ozel-Erol, M. Klein, and N. Chakraborty, "Lewis number effects on flame speed statistics in spherical turbulent premixed flames," Flow. Turbul. Combust. **106**, 1043–1063 (2021).
[55]N. Bouvet, F. Halter, C. Chauveau, and Y. Yoon, "On the effective Lewis number formulations for lean hydrogen/hydrocarbon/air mixtures," Int. J. Hydrogen Energy **38**, 5949–5960 (2013).
[56]F. B. Keil, M. Amzehnhoff, U. Ahmed, N. Chakraborty, and M. Klein, "Comparison of flame propagation statistics extracted from DNS based on simple and detailed chemistry part 1: Fundamental flame turbulence interaction," Energies **14**, 5548 (2021).
[57]F. C. Gouldin, K. N. C. Bray, and J. Y. Chen, "Chemical closure model for fractal flamelets," Combust. Flame **77**, 241–259 (1989).
[58]O. Chatakonda, E. R. Hawkes, A. J. Aspden, A. R. Kerstein, H. Kolla, and J. H. Chen, "On the fractal characteristics of low Damköhler number flames," Combust. Flame **160**, 2422–2433 (2013).
[59]V. A. Sabelnikov and A. N. Lipatnikov, "Bifractal nature of turbulent reaction waves at high Damkohler and Karlovitz numbers," Phys. Fluids **32**, 095118 (2020).
[60]N. Chakraborty and M. Klein, "A priori direct numerical simulation assessment of algebraic flame surface density models for turbulent premixed flames in the context of large eddy simulation," Phys. Fluids **20**, 085108 (2008).
[61]T. Dunstan, Y. Minamoto, N. Chakraborty, and N. Swaminathan, "Scalar dissipation rate modelling for large eddy simulation of turbulent premixed flames," Proc. Combust. Inst. **34**, 1193–1201 (2013).
[62]Y. Shim, S. Tanaka, M. Tanahashi, and T. Miyauchi, "Local structure and fractal characteristics of H_2-air turbulent premixed flame," Proc. Combust. Inst. **33**, 1455–1462 (2011).
[63]C. Meneveau and T. Poinsot, "Stretching and quenching of flamelets in premixed turbulent combustion," Combust. Flame **86**, 311–332 (1991).